

Article

# Investigations on the Wear Performance of Coated Tools in Machining UNS S32101 Duplex Stainless Steel

Vitor F. C. Sousa <sup>1</sup>, Francisco J. G. Silva <sup>1,2,\*</sup> , Ricardo Alexandre <sup>3</sup>, Gustavo Pinto <sup>1,2</sup> , Andresa Baptista <sup>1,2</sup>   
and José S. Fecheira <sup>1</sup>

<sup>1</sup> ISEP—School of Engineering, Polytechnic of Porto, Rua Dr. António Bernardino de Almeida 431, 4200-072 Porto, Portugal; vcris@isep.ipp.pt (V.F.C.S.); gflp@isep.ipp.pt (G.P.); absa@isep.ipp.pt (A.B.); jsf@isep.ipp.pt (J.S.F.)

<sup>2</sup> INEGI—Instituto de Ciência e Inovação em Engenharia Mecânica e Engenharia Industrial, Rua Dr. Roberto Frias 400, 4200-465 Porto, Portugal

<sup>3</sup> TeandM—Tecnologia, Engenharia e Materiais, S.A., Parque Industrial do Taveiro, Lotes 41–42, 3045-504 Taveiro, Portugal; ricardo@teandm.pt

\* Correspondence: fgs@isep.ipp.pt

**Abstract:** Due to their high mechanical property values and corrosion resistance, duplex stainless steels (DSSs) are used for a wide variety of industrial applications. DSSs are also selected for applications that require, especially, high corrosion resistance and overall good mechanical properties, such as in the naval and oil-gas exploration industries. The obtention of components made from these materials is quite problematic, as DSSs are considered difficult-to-machine alloys. In this work, the developed wear during milling of the UNS S32101 DSS alloy is presented, employing four types of milling tools with different geometries and coatings. The influence of feed rate and cutting length variations on the tools' wear and their performance was evaluated. The used tools had two and four flutes with different coatings: TiAlN, TiAlSiN and AlCrN. The cutting behavior of these tools was analyzed by collecting data regarding the cutting forces developed during machining and evaluating the machined surface quality for each tool. After testing, the tools were submitted to SEM analysis, enabling the identification of the wear mechanisms and quantification of flank wear, as well as identifying the early stages of the development of these mechanisms. A comparison of all the tested tools was made, determining that the TiAlSiN-coated tools produced highly satisfactory results, especially in terms of sustained flank wear.

**Keywords:** duplex stainless steel; milling; tool coatings; surface roughness; wear mechanisms



**Citation:** Sousa, V.F.C.; Silva, F.J.G.; Alexandre, R.; Pinto, G.; Baptista, A.; Fecheira, J.S. Investigations on the Wear Performance of Coated Tools in Machining UNS S32101 Duplex Stainless Steel. *Metals* **2022**, *12*, 896. <https://doi.org/10.3390/met12060896>

Academic Editor: Pavel Krakhmalev

Received: 26 March 2022

Accepted: 20 May 2022

Published: 25 May 2022

**Publisher's Note:** MDPI stays neutral with regard to jurisdictional claims in published maps and institutional affiliations.



**Copyright:** © 2022 by the authors. Licensee MDPI, Basel, Switzerland. This article is an open access article distributed under the terms and conditions of the Creative Commons Attribution (CC BY) license (<https://creativecommons.org/licenses/by/4.0/>).

## 1. Introduction

The use of duplex stainless steels (DSSs) in industries that benefit from the set of properties usually presented by these alloys, namely, high corrosion resistance and good mechanical properties, has deeply increased [1]. Thus, DSSs became appealing for many different applications in a wide range of industrial sectors [2–4], with these having better overall properties than most stainless steels, and even sometimes being presented as a viable alternative to some Ni-based alloys [5,6].

The machining process is heavily employed in the fabrication of high-quality and precision parts. Thus, the machining optimization of these alloys is quite appealing; however, the research about this topic is quite scarce. There are some authors that use techniques such as the Taguchi method, which is commonly employed in the optimization of machining processes [7–10]. These studies enable the identification of the machining parameters on the process, enabling optimization of production quality [11], material removal rate [12] and even generated cutting forces [13]. Another common method that can be employed to obtain information regarding the impact of a certain parameter is a multiple regression analysis [14,15], or response surface methodology (RSM), coupled with

an analysis of variance (ANOVA) [6]. These methods allow for the creation of predictive techniques that can be applied not only to surface roughness, as seen in [14], but to other parameters, such as the lowering of cutting forces or improving the material removal rate. This can be advantageous, as it avoids the execution of expensive and time-consuming machining tests.

Although parameter optimization is very important, from a process improvement standpoint, the tool being used is equally important, as it directly impacts process efficiency. Most machining tools for turning and milling, nowadays, are coated tools or coated carbide inserts [16,17]. These coatings have a wide range of benefits for machining applications that are well documented, such as an improved surface finish, tool longevity, reduction in cutting forces [18], lowering the coefficient of friction [19] and greatly improving the wear resistance of coated tools and surfaces [20–22]. Tool coatings are usually obtained either by physical vapor deposition (PVD) or by chemical vapor deposition (CVD). Each of the processes produces different kinds of coatings with different properties and structures, as they use different methods to achieve the deposited films [23–26]. There are many studies on the comparison of coatings for the machining of various alloys, especially hard-to-machine alloys, with comparisons between PVD and CVD coatings being commonly made as researchers try to find advantages of one type of coating over the other and, also, try to optimize/improve the machining process by using coated tools [27–29]. These studies are very useful, as the coating's properties greatly affect the machining performance, with the coating's mechanical properties, structure, microstructure and residual stresses having a great influence on the machining process, stressing the importance of correct coating selection [30–33].

Cutting forces that are generated during the process provide valuable information regarding the overall process' state, thus enabling machining process optimization. This means that cutting force data provide a way to monitor the process or identify certain aspects that can be improved in the machining process. The knowledge of these cutting forces can be used to monitor tool behavior [34,35] and give information on optimal machining parameters [36,37], thus enabling the improvement of the machining process, either by parameter optimization, by improving tool life or even by helping with the development of new machining tool technology [38,39]. There are different methods for determining cutting forces, either by using a direct or indirect approach [40–43]. Further regarding machining process optimization, the analysis of the wear mechanisms that cutting tools present also brings many advantages, enabling machining process optimization by improving tool life, creating new geometries more adequate for the machining of certain materials and even optimizing the coatings of these tools by providing information on the right coating to use for a certain application. Analysis of these wear mechanisms provides valuable information that can be used for parameter adjustment as well [44]. There are studies made in this regard, focused on DSS, with common wear mechanisms being registered, such as abrasion and adhesive wear, due to the high strength of the material and high friction values reached during machining of these alloys [45–47]. Knowledge about tool wear behavior is highly important [48], as it provides information on what is occurring during machining, enabling for a decision-making process that is focused on improving the process. Either by implementing a new cooling method or adjusting machining parameters, this knowledge also enables the selection of the right tool for the job (prioritizing tool life, surface roughness and overall process efficiency), considering tool geometry and coating [45,49–51]

In this work, the wear behavior and machining performance of milling tools used in finishing operations of the UNS S32101 DSS alloy is presented. Four tools with differing geometries and coatings were used, namely, TiAlN, TiAlSiN and AlCrN coatings. Two of the tested tools were coated with AlCrN, one having two flutes and the other four flutes, as this coating is recommended for the machining of DSS alloys. The machining parameters were also varied, testing two values of cutting length and three values of feed rate. The influence of these coatings, tool geometries and machining parameter variations on the wear

behavior and production quality of the tools was assessed. This assessment was performed by subjecting the tools to SEM analysis, measuring flank wear (VB) and identifying the sustained wear mechanisms. The machined surface roughness was also evaluated to characterize this influence. The obtained results are presented in this manuscript, with one section dedicated to each of the performed analyses (surface roughness assessment, flank wear measurement and wear mechanism analysis). The authors hope that with these results, the gap regarding the machining of these alloys can be somewhat filled, contributing information that could be relevant when it comes to the optimization of the machining of these alloys.

## 2. Materials and Methods

In this section, the various materials and methods employed during this work will be presented in various subsections, as to provide a clear understanding of what was used throughout the various work phases.

### 2.1. Materials

#### 2.1.1. Employed Tools

In this work, four tool types were used to machine the DSS alloy. The tools' substrate was cemented carbide WC-Co grade 6110, provided by INOVATOOLS, S.A. (Leiria, Portugal). This cemented carbide grade presented as micro-grain, with a measurement of about 0.3  $\mu\text{m}$ , and used 6% Co (wt.) as a binder. The tools' substrate was ground, yet the patterns left by this process were seen in the tools' surfaces, even after the deposition process. Regarding the tools' dimensions, all the produced tools were 4 mm in diameter and had a total length of 68 mm. As this study aimed to compare the influence of different coatings as well as different tool geometries in the wear mechanism suffered during machining tests, four tools with different geometries were produced and were coated with three different coatings, TiAlN, TiAlSiN and AlCrN. After production, the tools were subjected to an ultrasonic bath using acetone for 10 min; after this first bath, the tools underwent a second one for 5 min. The acetone was changed between the baths. These tools were coated with three types of PVD coatings, the TiAlN, TiAlSiN and AlCrN coatings. This enabled the comparison of the wear behavior and machining performance of these coatings by creating four different tools, as seen in Table 1.

**Table 1.** Tools created for the machining of UNS S32101.

Tool Ref.	Tool Geometry	Number of Flutes/Edges	Rake Angle	Relief Angle
T1	Flat end-mill	2	30°	10°
T2	End-mill with a 45° chamfer, 0.08 mm from the cutting edge	4	35°	10°
T3	Flat end-mill	4	40°	5°
T4	End-mill with a 0.2 mm corner radius	4	35°	10°

Regarding the deposition of these coatings, CemeCon CC800/9ML PVD unbalanced magnetron sputtering equipment provided with four target holders was used. After the cleaning process, the tools were assembled in a holder and placed inside the equipment. To ensure that the coatings were deposited onto the tools' surfaces as homogeneously as possible, the tool holders were rotated at a speed of 1 rpm during the process. The coating process was similar for the TiAlN and TiAlSiN coatings, with the use of four similar targets. In the case of the AlCrN coating, four targets were also used, two being composed of 100% Cr and the other two of 100% Al. These targets were distributed alternately inside the reactor, resulting in the deposition of alternating layers of Cr and Al. Thin, alternating layers of Al and Cr were achieved on the T1 and T3 tools. The set of parameters used for the deposition of the mentioned coatings can be observed in Table 2. During the deposition

of the various tool sets, flat substrates were placed inside the deposition chamber to create a sample that could be used to determine the coatings' mechanical properties.

**Table 2.** TiAlN, TiAlSiN and AlCrN PVD coatings' deposition parameters.

Parameters	TiAlN Coating	TiAlSiN Coating	AlCrN Coating
Deposition time (min.)	240	240	240
Reactor gases	Ar <sup>+</sup> + Kr + N <sub>2</sub>	Ar <sup>+</sup> + Kr + N <sub>2</sub>	Ar <sup>+</sup> + Kr + N <sub>2</sub>
Target material	4TiAl 40/60	4TiAlSi 38/57/5	2Al + 2Cr
Pressure (mPa)	580	580	580
Temperature (°C)	450	450	450
Bias (V)	−110	−110	−110
Target current density (A/cm <sup>2</sup> )	20	20	20
Holder rotational speed (rpm)	1	1	1

These parameters have been selected based on previous successful experiments carried out in similar substrates. After deposition, all the tools were packed carefully, avoiding the handling of the tools' cutting areas.

### 2.1.2. Machined Material

The machined material is a duplex stainless steel, UNS S32101, which was provided as a round bar that was 75 mm in diameter. Regarding this material's mechanical properties, it has a yield strength of 450 MPa and ultimate tensile strength of 650 MPa, following the information provided by the material's manufacturer (Outokumpu). This steel has an average hardness of  $280 \pm 20$  HV5, and its chemical composition was provided by the manufacturer and can be observed in Table 3. The hardness values were confirmed by performing ten measurements with universal hardness testing equipment, the EMCO M4U, using a 5 kgf and a dwell time of 30 s. The hardness values were in accordance with those present in the material's data sheet (290 HV5), exhibiting a slight deviation.

**Table 3.** Chemical composition (wt%) of the DSS, UNS S32101.

C	Mn	Cu	Cr	Ni	Mo	N
0.03	5.0	0.3	21.5	1.5	0.3	0.22

## 2.2. Methods

### 2.2.1. Coatings' Thickness Analysis

The coating thickness analysis was carried out on cross-sections of samples, obtained as described in the previous section. The coating thickness measurement was performed using a FEI QUANTA 400 FEG scanning electron microscope (SEM), provided with an EDAX Genesis energy dispersive X-ray spectroscopy microanalysis system. The same range of magnifications were used in all the pictures obtained by the SEM, allowing for a greater ease of comparison of phenomena between different samples. The values for coating thickness were obtained by calculating the mean value of the measurements registered during SEM analysis. A total of six different measurements across different zones for each of the coated tools were performed. EDS analyses were carried out with a beam potential of 15 kV; however, this was sporadically reduced to 10 kV to decrease the volume of interaction and reduce noise in the spectra. Although the reading accuracy of the EDS analyses as a quantitative evaluation is not the best, it was also used to confirm the chemical composition of the coatings, which was sufficient for this purpose and avoided employment of more costly technologies.

## 2.2.2. Machining Tests

### Machining Strategy

The machining tests were performed in a HAAS VF2 CNC milling center, capable of reaching 10,000 rpm and having a maximum power of 20 kW. A strategy was devised to machine the material: as its geometry was round, the tools would machine the material in a spiral motion, going from the outside of the raw material to its center. The machining tests were performed using a water-miscible cutting fluid projected externally (5% oil in water); furthermore, a set of parameters were chosen by considering the optimal values for machining operations that were suggested by the tools' substrate provider. The machining parameter values were determined and applied to all the tools to enable the comparison of their wear behavior and cutting performance. These parameters can be observed in Table 4. To ensure the repeatability of the tests, each milling test was performed three times for each set of cutting conditions to produce a greater number of results regarding wear mechanisms and the surface roughness of the machined surface, thus improving the consistency of the obtained data. Regarding the machining parameters, a constant radial depth of cut and vertical depth of cut were used, these being 3 mm and 0.08 mm, respectively. Furthermore, a constant cutting speed of 60 m/min was used. To evaluate the influence of feed on the machined surface roughness and on the tools' wear, this parameter was varied by 25% by creating test conditions that employed 75% and 125% of the recommended feed value, which was 479 mm/min. To determine the best cutting length to carry out this comparative experimental work, the cutting force analysis was used. For this purpose, one of each fabricated tool was used for the machining of the material, using the strategy and parameters described above. For this preliminary test, a cutting length of 25 m was used in the procedure described in detail (mentioning the equipment) in the following subsection.

**Table 4.** Parameters used in the machining tests.

Sample	Coating	Cutting Speed	Number of Edges	Feed Rate	Depth of Cut	Radial Depth of Cut	Cutting Length
Reference	Type	mm/min		mm/min	mm	mm	m
T1L4F75	AlCrN	60	2	359.25	0.08	3	4
T1L2F75	AlCrN	60	2	359.25	0.08	3	2
T1L4F100	AlCrN	60	2	479	0.08	3	4
T1L2F100	AlCrN	60	2	479	0.08	3	2
T1L4F125	AlCrN	60	2	598.25	0.08	3	4
T1L2F125	AlCrN	60	2	598.25	0.08	3	2
T2L4F75	TiAlN	60	4	359.25	0.08	3	4
T2L2F75	TiAlN	60	4	359.25	0.08	3	2
T2L4F100	TiAlN	60	4	479	0.08	3	4
T2L2F100	TiAlN	60	4	479	0.08	3	2
T2L4F125	TiAlN	60	4	598.25	0.08	3	4
T2L2F125	TiAlN	60	4	598.25	0.08	3	2
T3L4F75	AlCrN	60	4	359.25	0.08	3	4
T3L2F75	AlCrN	60	4	359.25	0.08	3	2
T3L4F100	AlCrN	60	4	479	0.08	3	4
T3L2F100	AlCrN	60	4	479	0.08	3	2
T3L4F125	AlCrN	60	4	598.25	0.08	3	4
T3L2F125	AlCrN	60	4	598.25	0.08	3	2
T4L4F75	TiAlSiN	60	4	359.25	0.08	3	4
T4L2F75	TiAlSiN	60	4	359.25	0.08	3	2
T4L4F100	TiAlSiN	60	4	479	0.08	3	4
T4L2F100	TiAlSiN	60	4	479	0.08	3	2
T4L4F125	TiAlSiN	60	4	598.25	0.08	3	4
T4L2F125	TiAlSiN	60	4	598.25	0.08	3	2

### Cutting Force Analysis

Cutting forces developed during machining can provide valuable information regarding the tools' wear. To acquire these cutting forces, a 4-component KISTLER 9171A dynamometer was used, coupled to a KISTLER 5697A1 data acquisition system, which allowed to record the cutting forces developed in X, Y and Z axes, as well as the developed torque ( $M_z$ ), through appropriate software supplied with the dynamometer. The equipment was coupled to the spindle of the CNC machining center, having then the appropriate clamping system for placing the tool. The acquisition rate of the developed forces was selected according to the spindle's rotation speed, and the force of all the cutting edges of the tool at each rotation was registered. The results were collected and analyzed, enabling the identification of any increase or abnormal behavior of the cutting forces that could be caused by wear phenomena on the tool.

### Machining Test Parameters

With the determined cutting lengths, the wear mechanisms that these tools suffer during machining could be evaluated. The main concern was to identify the early wear phenomena as well as its evolution under these cutting conditions, and not to determine the lifespan of the tools. The determined parameters for each test can be observed in Table 4, including the sample reference used for each of the tested tools.

Three tools were used for each of the conditions presented above. The use of lubricant during the machining tests caused difficulties in the analysis of the tools' surfaces. Thus, all the tools underwent one ultrasonic bath using acetone for 5 min to remove the presence of lubricant on the areas where SEM analysis was to be performed. This bath had a short duration to prevent the eventual removal of adhered material or sections of coating (near detachment). The surface roughness of the material was also assessed after each machining test.

#### 2.2.3. Surface Roughness Test

Surface roughness evaluation is very important in the machining process, as it is closely related to machining performance, tool wear and process stability. In this work, the material's machined surface roughness was characterized in two directions: radial and tangential (machining direction). To assess this parameter, surface roughness tests were conducted using a MAHR PERTHOMETER M2 profilometer, following the standard procedure described in DIN EN ISO 4288/ASME b461. Each test covered a length of 5.6 mm, corresponding to seven segments of the cut-off value (0.8 mm), with the first and last value being ignored due to the acceleration and deceleration of the probe arm. For the surface roughness analysis, the following parameters were considered: arithmetic mean roughness ( $R_a$ ) and the maximum roughness ( $R_{max}$ ). The R profile was also analyzed to identify any sharp peaks in the surface roughness values and other phenomena.

#### 2.2.4. Tool Wear Analysis

After machining, all the tools were subjected to SEM analyses to access the amount of wear that these tools sustained and to identify the wear mechanisms developed on the various tools during machining. To access the wear, the values for flank wear were measured ( $VB$ ) according to the ISO 8688-2:1986 standard [52]. Furthermore, the values of  $VB$  that were presented were the mean values for each tool for each of the test conditions.

A reference for the tool analysis was created and can be observed in Figure 1; both the rake face and clearance face were analyzed, identifying the wear mechanisms that were present and measuring the flank wear ( $VB$ ) on the clearance face of the tested tools.

The numerations observed in Figure 1 were adopted in the identification of the SEM images, with the rake face and clearance face being identified with RF and CF, respectively, identifying the edge under analysis as presented in Figure 1. Additionally, since three tools were used for each of the test conditions, an identification number (ranging from 01 to 03) was added at the end of the image reference.

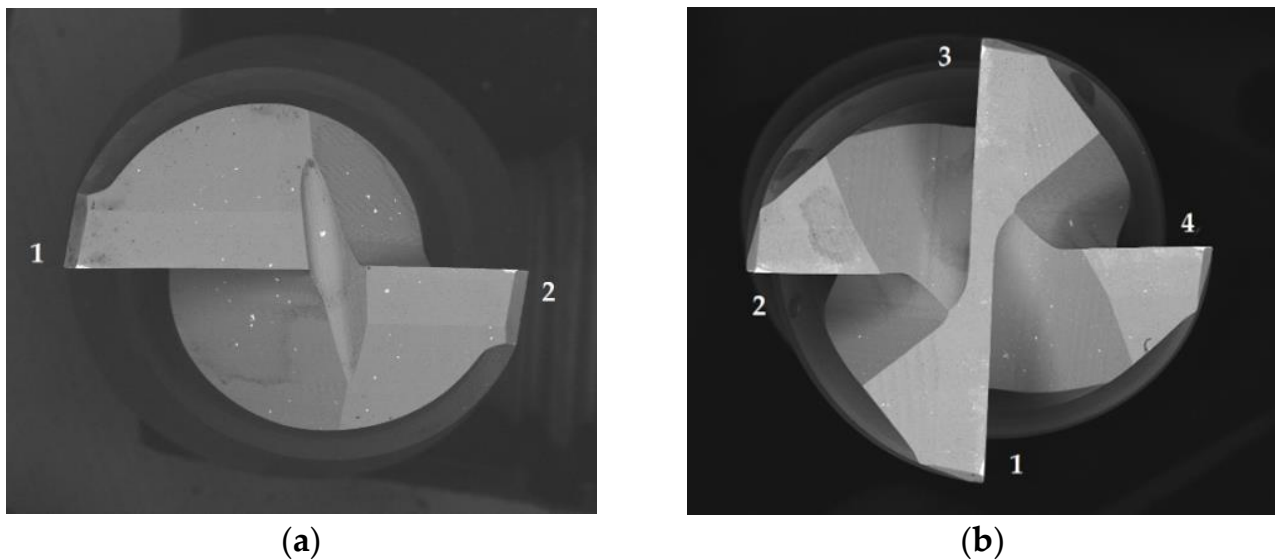


**Figure 1.** Reference used for the SEM analysis of the end-mills with (a) two cutting edges, and (b) four cutting edges.

### 3. Results and Discussion

In this section, the results obtained from all the tests and analyses are presented, organized and divided into various subchapters.

#### 3.1. Coatings' Characterization

For the coatings' characterization, the thickness of the three applied coatings was analyzed by preparing the unused tools for SEM analysis. Both the T1 and T3 tools were considered in the characterization of the AlCrN coating, as they were coated with the same coating using the same deposition parameters. Regarding the thickness measurements, these were performed in the same area for all the tested tools. Thickness values were obtained near each tool's rake and clearance face (obtained from the tools' cross-sections). The average thickness value was then determined. It is worthy to note that there were no significant changes detected for the analyzed coatings' thicknesses.

The average thickness values registered for each of the coatings can be observed in Table 5.

**Table 5.** Average thickness values for the analyzed coatings.

Coating	Thickness ( $\mu\text{m}$ )
TiAlN	$2.812 \pm 0.121$
TiAlSiN	$2.799 \pm 0.163$
AlCrN	$2.965 \pm 0.227$

Although the AlCrN coating is a multi-layered coating, in the polished samples the interface between layers was not observed. This was due to the polishing process itself, as it smoothed the sample's cross-section, homogenizing the coating and making it look like a monolithic coating. However, if the coating was fractured, this multi-layered structure was observed, as seen in Figure 2a. Also in Figure 2, SEM measurements of the TiAlSiN coating thickness can be observed. This is an example of a measurement performed for all the coatings' thicknesses. In Figure 2a, the Al layers are the lighter ones, whereas the Cr-rich layers are the darker ones. Regarding their thickness, due to the SEM equipment's limitations, this was not determined.

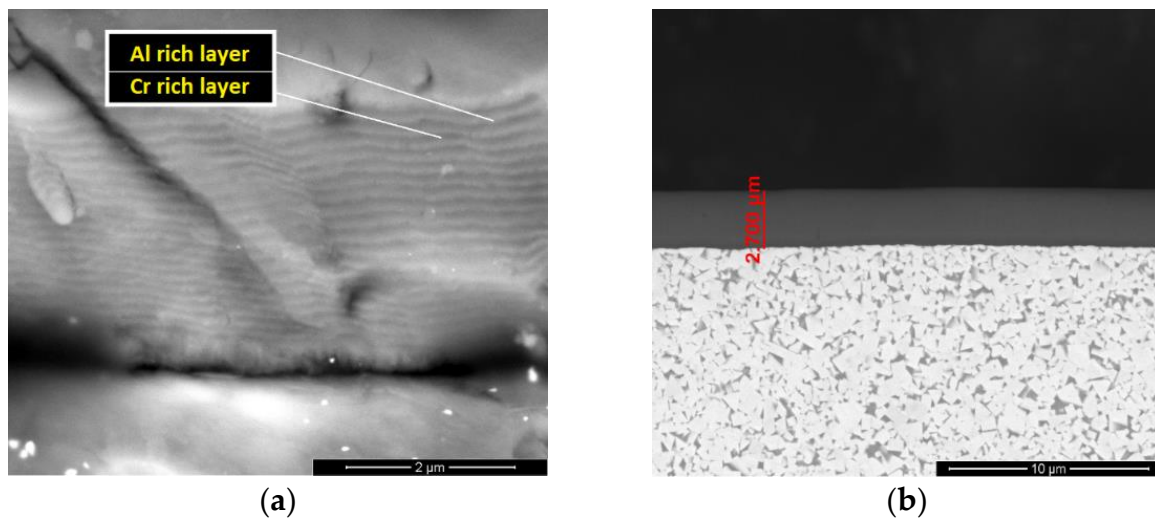


**Figure 2.** Coatings' thickness analysis: multi-layered structure of the AlCrN coating (a); measurement of TiAlSiN (b).

The coatings' mechanical properties were also evaluated, namely, hardness and the Young's modulus, by conducting ultra-micro hardness tests on the TiAlN, TiAlSiN and AlCrN coatings using a dynamic ultra-micro hardness tester, the Fischerscope H100. As previously mentioned, the coatings were deposited onto flat substrate samples that were coated simultaneously with the tools. Ten tests were conducted on each of the deposited coatings, determining values for hardness and the reduced Young's modulus. The average of these values was calculated and is presented in Table 6. In Figure 3, the hardness values of the coatings are presented as a column graph, comparing these with the hardness value of the base material.

**Table 6.** Average hardness, Young's modulus, H/E and  $H^3/E^2$  ratio values obtained for the produced coatings.

Coating	Hardness (H)—GPa	Reduced Young's Modulus (Er)—GPa	H/E	$H^3/E^2$
TiAlN	$22.9 \pm 1.2$	$312 \pm 9$	0.073	0.123
TiAlSiN	$21.6 \pm 0.9$	$266 \pm 7$	0.081	0.142
AlCrN	$36.8 \pm 2.1$	$335 \pm 5$	0.11	0.395

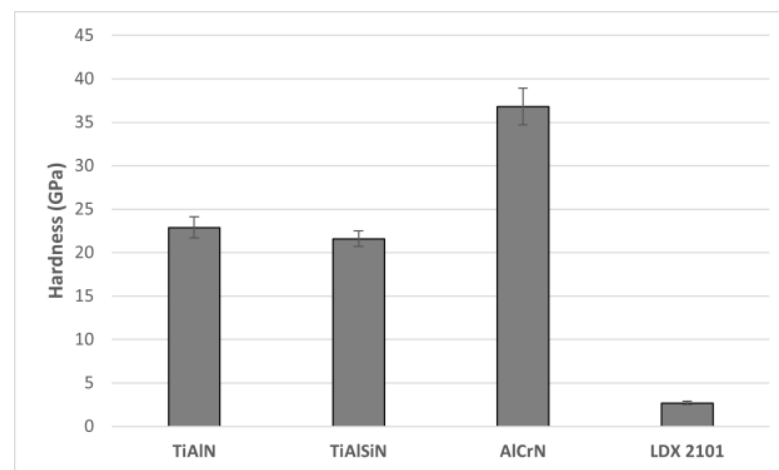


**Figure 3.** Hardness values of the tested coatings and base material (UNS S32101).

As seen in Table 6, the  $H/E$  and  $H^3/E^2$  ratios are displayed. These ratios provide valuable information regarding the coatings' wear behavior [53], with the  $H/E$  ratio being a good indicator of the coating's wear resistance, with higher values being preferred (closer to 1; however, the presented values are quite satisfactory for all analyzed coatings). The  $H^3/E^2$  ratio is related to the coating's ability to resist plastic deformation, which impacts the coating's wear behavior as well [54] (for this ratio, the higher value is also preferred, with ratios closer to 1 indicating very good plastic deformation resistance).

Still regarding the coating's wear behavior, another indicator of this is the ratio between the Young's modulus value of the coating and the substrate. Usually, a higher  $E$  value in the substrate is preferred (when compared to the coating's  $E$  value), as this can delay the onset of plastic deformation in the substrate and avoid subsequent coating cracking and chipping [55]; as such, lower values of this ratio are preferred. Substrate/coating systems that have this ratio closer to 1 are more susceptible to phenomena such as cracking and coating delamination. The substrate's Young's modulus was determined to be 611 GPa (average value). In Table 7, the ratio between the coatings ( $E_c$ ) and the substrate's ( $E_s$ ) Young's modulus value can be observed.

**Table 7.**  $E_c/E_s$  ratio determined for each of the tested coatings.

Coating	$E_c/E_s$
TiAlN	0.511
TiAlSiN	0.435
AlCrN	0.581

### 3.2. Cutting Force Analysis

Cutting forces provide valuable information regarding the machining process, primarily about process stability and tool wear. Using the methodology presented in the previous chapter, cutting forces were also registered during all the conducted tests; however, due to the used parameters, primarily a low depth of cut, the cutting forces produced did not present high values.

Analyzing the cutting force graphs obtained from each of the conducted tests, a common trend was noticed. Independent of feed rate, the cutting forces registered an increase in value for the  $F_x$ ,  $F_y$  and  $F_z$  components, with the increase in the  $F_z$  component being quite significant for all the cases. This increase was registered at around 2 m of the cutting length for all the tested tools. It was also registered that the values for these components increased until the end of the test, at 4 m of the cutting length.

This increase in cutting force value may be attributed to the wear sustained by the cutting tools; however, this cutting force value variation was quite low (as previously mentioned). These low values were attributed to the selected cutting parameters, and more concretely, the low value of the axial depth of cut. Due to this fact, these values were omitted in further analyses.

### 3.3. Surface Roughness Analysis

In this section, the surface roughness analysis results are presented, showing the average  $R_a$  values for the tangential and radial measurement directions, as any deviation between these values of roughness indicates instability during machining, usually presenting as a higher level of vibration during the cutting operation. These results are divided into subsections, one for each of the tested tools, with an extra subsection where the comparison between the tools, regarding the roughness values, is presented. The adopted procedure is described in detail in Section 2.

#### 3.3.1. T1—Produced Surface Roughness

The average surface roughness values that were measured in the material machined with the T1 tools are presented in Table 8. These were used to create surface graphs to

depict the surface roughness variation for all the tested conditions. Table 8 adopted the tool reference described in Section 2.

**Table 8.** Average surface roughness values, measured in the radial and tangential directions for the tests conducted with T1.

Tool Ref.	Ra (Radial Direction) ( $\mu\text{m}$ )	Ra (Tangential Direction) ( $\mu\text{m}$ )
T1L2F75	$0.193 \pm 0.015$	$0.182 \pm 0.019$
T1L4F75	$0.325 \pm 0.021$	$0.345 \pm 0.031$
T1L2F100	$0.219 \pm 0.019$	$0.223 \pm 0.011$
T1L4F100	$0.394 \pm 0.033$	$0.389 \pm 0.016$
T1L2F125	$0.254 \pm 0.012$	$0.327 \pm 0.044$
T1L4F125	$0.481 \pm 0.036$	$0.492 \pm 0.056$

From the values presented in Table 8, it was observed that the values measured in the tangential and radial directions are very similar. However, this deviation was not significant. Thus, it can be concluded that in this case, the machining process itself was stable.

By analyzing the surface roughness values measured for both directions, it was observed that they follow a similar trend of rising with the cutting length; i.e., tests conducted with the tool with the 2-m cutting length produced the best results in terms of surface roughness. This was due to the tool's wear, which was aggravated for higher cutting lengths. Another parameter that seemed to influence the surface roughness of the material was the feed rate, as it was observed for lower feed rates that the tools produce a better surface quality. From the lowest feed rate value to the original, a slight increase in surface roughness was registered; however, for feed rates of 125%, the surface roughness that was produced was the highest registered, with the maximum produced under the condition of 4 m of cutting length while using 125% of the original feed rate (T1L4F125).

### 3.3.2. T2—Produced Surface Roughness

Regarding the Ra values obtained for the tests conducted using T2 tools, these can be observed in Table 9.

**Table 9.** Average surface roughness values, measured in the radial and tangential directions for the tests conducted with T2.

Tool Ref.	Ra (Radial Direction) ( $\mu\text{m}$ )	Ra (Tangential Direction) ( $\mu\text{m}$ )
T2L2F75	$0.291 \pm 0.018$	$0.260 \pm 0.012$
T2L4F75	$0.401 \pm 0.026$	$0.436 \pm 0.021$
T2L2F100	$0.325 \pm 0.017$	$0.301 \pm 0.015$
T2L4F100	$0.413 \pm 0.031$	$0.405 \pm 0.026$
T2L2F125	$0.409 \pm 0.019$	$0.409 \pm 0.014$
T2L4F125	$0.505 \pm 0.037$	$0.477 \pm 0.022$

As seen from Table 9, the Ra values measured in the tangential and radial directions were very similar, meaning that there were no excessive vibrations produced during the machining tests. From the surface roughness values analysis, it was observed that, as seen from the results of the tests using T1, the surface roughness was lower for lower feed values. Furthermore, the cutting length also had a clear influence in the machined material's surface quality, registering a clear increase in surface roughness for the tests conducted at a 4 m cutting length. Once again, the highest surface roughness value was obtained under the condition of a 4-m cutting length and higher feed rate value (125%). It is also worth noting that the increase in surface roughness value from a 75% to 100% feed rate was less accentuated than the increase registered from a 100% to 125% feed rate. This was a similar behavior to that observed in the tests conducted with T1.

### 3.3.3. T3—Produced Surface Roughness

In Table 10, the average calculated values of Ra from the surface roughness measurements conducted on the machined material (using T3 tools) can be observed.

**Table 10.** Average surface roughness values, measured in the radial and tangential directions for the tests conducted with T3.

Tool Ref.	Ra (Radial Direction) ( $\mu\text{m}$ )	Ra (Tangential Direction) ( $\mu\text{m}$ )
T3L2F75	$0.234 \pm 0.016$	$0.206 \pm 0.013$
T3L4F75	$0.270 \pm 0.019$	$0.273 \pm 0.029$
T3L2F100	$0.209 \pm 0.009$	$0.211 \pm 0.021$
T3L4F100	$0.299 \pm 0.011$	$0.295 \pm 0.031$
T3L2F125	$0.172 \pm 0.012$	$0.190 \pm 0.012$
T3L4F125	$0.228 \pm 0.022$	$0.228 \pm 0.025$

Comparing the values shown in Table 10 to those obtained from the tests conducted with the previous tools (T1 and T2), it was observed that the Ra values were quite lower for the tests performed with the T3 tools. Analyzing the variation of Ra values with the different test conditions, similarly to the previously presented results, showed that the surface roughness values tended to increase for higher cutting lengths. However, there was a different trend noticed with the feed variation. Unlike what was observed for the other test conditions, a significant decrease in surface roughness values were registered for higher feed rate test conditions (125%), with these producing, by far, the best surface quality registered to this point. In this case, the worst surface quality was obtained under the test condition of 4 m of cutting length while using the original feed rate (T3L4F100). The lowest value of Ra was obtained under the condition of a 2-m cutting length, using 125% of the original feed rate (T3L2F125).

### 3.3.4. T4—Produced Surface Roughness

In this subsection, the surface roughness results for the machining tests conducted with T4 tools are presented. The average values of the measured Ra (in both radial and tangential directions) parameter can be observed in Table 11. As seen in the previous subsections regarding the surface roughness results obtained using the different tools, surface roughness varies with the cutting length and feed rate values.

**Table 11.** Average surface roughness values, measured in the radial and tangential directions for the tests conducted with T4.

Tool Ref.	Ra (Radial Direction) ( $\mu\text{m}$ )	Ra (Tangential Direction) ( $\mu\text{m}$ )
T4L2F75	$0.194 \pm 0.018$	$0.175 \pm 0.011$
T4L4F75	$0.253 \pm 0.025$	$0.253 \pm 0.018$
T4L2F100	$0.259 \pm 0.016$	$0.247 \pm 0.011$
T4L4F100	$0.274 \pm 0.019$	$0.284 \pm 0.016$
T4L2F125	$0.250 \pm 0.022$	$0.270 \pm 0.014$
T4L4F125	$0.284 \pm 0.033$	$0.323 \pm 0.021$

From the analysis of Table 11, it was concluded that the process was stable, as the values for Ra measured in the tangential and radial directions did not deviate significantly from each other. The variation in Ra values for different parameters was like the variation observed in the tests conducted with T1 and T2 tools. Once again, the 2-m cutting length test condition produced the best surface roughness quality, with this deteriorating with the increase in this parameter, as observed in all the analyzed tools. Regarding the variation of Ra with the feed rate, as previously mentioned, it was observed that the lowest Ra value was obtained by using lower feed rate values, with the surface quality quickly deteriorating with the increase in feed rate.

### 3.4. Flank Wear Measurements

The wear measured in the tools' flanks for each test condition is presented in this section in numerical form, presenting the average values of flank wear, as well as in graphical form, enabling for a clear perception on how this wear varies with the machining parameters. These values were measured on the clearance faces of all the tested tools, following the standard ISO 8688-2:1989 [52], as mentioned in Section 2. As in the previous Section 3.3., these values are in different subsections, one for each of the analyzed tools, with an extra section dedicated to the comparison of the flank wear values obtained.

#### 3.4.1. T1—Flank Wear Measurement

In this subsection, the wear measurement values, performed on the clearance faces of all the tested T1 tools, are presented in Table 12.

**Table 12.** VB values obtained from measurements performed on the clearance faces of T1 tools.

Tool Ref.	Flank Wear, VB ( $\mu\text{m}$ )
T1L2F75	$14.22 \pm 1.05$
T1L4F75	$18.34 \pm 1.16$
T1L2F100	$9.670 \pm 0.78$
T1L4F100	$12.27 \pm 0.98$
T1L2F125	$23.32 \pm 1.84$
T1L4F125	$25.20 \pm 1.76$

From the values presented in Table 12, it was concluded that the increase in cutting length caused a slight increase in flank wear. However, it was a very small increase, especially when compared to the variation in flank wear that was observed with feed variation. For the lower feed rate, the tools presented slightly more flank wear than those that were tested at a 100% feed rate. There was also an increase in flank wear for higher feed rates; however, these feed rates produced the most severe wear, with high values of flank wear being registered at these values of feed rate when 2- and 4-m cutting lengths were used. In terms of a less amount of wear, this was obtained under the original cutting condition, with the lowest amount of wear being registered for T1L2F100 and followed by T1L4F100, indicating that the machining parameters were well defined for this tool in terms of wear behavior.

#### 3.4.2. T2—Flank Wear Measurement

In Table 13, the average flank wear values obtained from measurements performed on the clearance faces of the T2 tools are presented.

**Table 13.** VB values obtained from measurements performed on the clearance faces of T2 tools.

Tool Ref.	Flank Wear, VB ( $\mu\text{m}$ )
T2L2F75	$8.380 \pm 0.69$
T2L4F75	$13.18 \pm 1.12$
T2L2F100	$7.040 \pm 0.24$
T2L4F100	$10.01 \pm 0.98$
T2L2F125	$13.21 \pm 1.12$
T2L4F125	$25.12 \pm 1.05$

As seen in the analysis of T1, the variation of the flank wear for the T2 tools was deeply influenced by the feed rate, increasing slightly under the 75% feed rate condition, and registering a significant increase under the 125% feed rate condition. Once again, the original values of feed rate produced better results in terms of tool wear, even at 4 m of cutting length. The variation in cutting length induced a higher tool wear for the 125% feed

rate condition, registering a significant increase, whereas in the case of the 75% and 100% feed rates, the cutting length did not appear to influence the tools' wear so severely.

#### 3.4.3. T3—Flank Wear Measurement

In Table 14, the average VB values that were measured on the clearance faces of the T2 tools are presented.

**Table 14.** VB values obtained from measurements performed on the clearance faces of T3 tools.

Tool Ref.	Flank Wear, VB ( $\mu\text{m}$ )
T3L2F75	11.72 $\pm$ 1.06
T3L4F75	12.54 $\pm$ 0.85
T3L2F100	14.17 $\pm$ 1.26
T3L4F100	16.26 $\pm$ 1.55
T3L2F125	6.820 $\pm$ 0.55
T3L4F125	8.570 $\pm$ 0.19

Observing the values presented in Table 13, it was concluded that T3 tools did not suffer wear in the same manner as the T1 and T2 tools. In fact, the behavior of the wear was like the variation of the Ra values of the studied tools, where T1 and T2 tools produced better results at lower feed rates in terms of surface roughness and even wear (as the wear sustained at a 75% feed rate is very similar to that sustained at 100%). However, in the case of T3 tools, it was observed that the best results in terms of wear were obtained at higher feed rates (125%). This can be compared to the results obtained from the surface roughness analysis of this tool, as the best surface quality was also achieved at higher feed rates [11,14].

In terms of amount of wear, a slight decrease in wear for the lowest feed rate value was observed, albeit very similar to the wear sustained at the original feed rate. However, for higher feed rate values, the wear was significantly lower. This fact, coupled with the results obtained from the surface roughness analysis, indicates that this tool has a high-performance for higher feed values, producing low surface roughness values while sustaining less flank wear [11]. Regarding the flank wear variation with the increasing cutting length, as expected, these values rose slightly for higher cutting lengths; however, the main influence in flank wear for this case seemed to be the feed rate.

#### 3.4.4. T4—Flank Wear Measurement

The flank wear analysis for the final tool type, T4, is presented in this subsection. Average flank wear values, measured on the clearance faces of these tools and tested for all different conditions, can be observed in Table 15.

**Table 15.** VB values obtained from measurements performed on the clearance faces of T4 tools.

Tool Ref.	Flank Wear, VB ( $\mu\text{m}$ )
T4L2F75	6.710 $\pm$ 0.36
T4L4F75	13.71 $\pm$ 0.74
T4L2F100	10.47 $\pm$ 0.66
T4L4F100	18.80 $\pm$ 1.16
T4L2F125	4.770 $\pm$ 0.22
T4L4F125	5.830 $\pm$ 0.65

In this case, the flank wear increased with cutting length, especially at 75% and 100% feed rate values. There was an influence in wear registered for the 125% feed rate; however, the registered increase was very slight. In terms of flank wear variation coupled with the feed rate, as seen in the previously analyzed tool (T3), the lowest values of flank wear were registered for higher feed rates; however, the wear values registered at the lowest feed rate

condition were like those obtained at the 125% feed rate, especially for the test conducted with 2 m of cutting length. The highest amount of wear was produced at a 100% feed rate value at 4 m of cutting length, which impacted the overall quality of the machined surface [11] as seen in the previous section, and was followed by T4L2F100. It is also worth noting that the produced values of flank wear were low when compared to those obtained in T1 and T2, indicating that this tool has good wear performance when machining this type of material, even at higher feed rates.

### 3.5. Analysis of the Wear Mechanisms

In the present section, a detailed analysis of the wear mechanisms sustained by the different tools is presented. Following the same method of presentation seen in the previous section, the different wear mechanisms are presented for each tool, presenting a comparison as well between the wear observed in the SEM images and the values presented in the previous subsection. Furthermore, at the end of this section, an additional subsection is presented that gives a summary of the wear mechanisms that were analyzed for each tool, identifying common trends in terms of wear mechanisms and wear behavior.

#### 3.5.1. T1—Wear Mechanism Analysis

Here, the images taken from the SEM analysis regarding the T1 tools are presented. The main types of wear that these tools sustained were abrasive wear, coating cracking and delamination, exhibiting some adhesion of machined material. As expected, there was an influence on wear severity caused by the increase in cutting length, as can be observed in Figure 4.

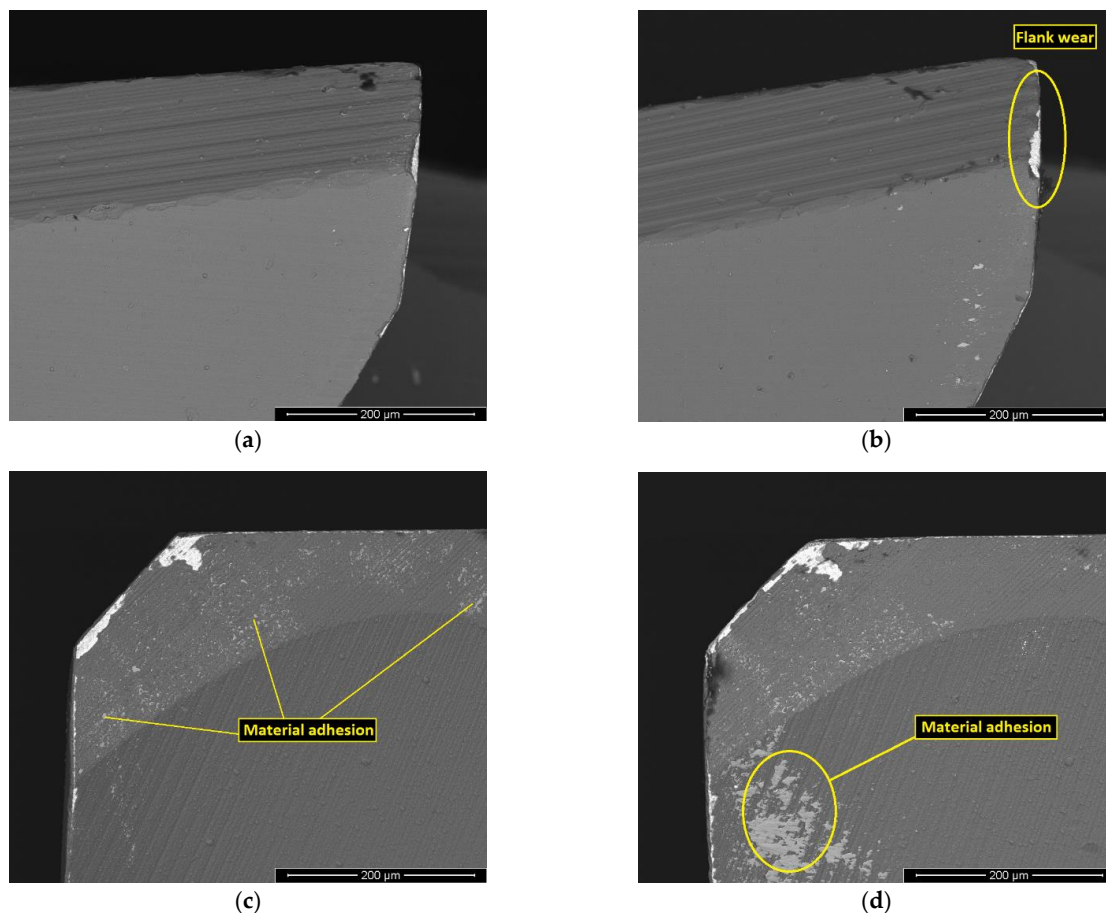


**Figure 4.** Clearance face, with a 500× magnification, of the T1L2F100 (a) and T1L4F100 (b) tools, and rake face, with a 500× magnification, of the T1L2F100 (c) and T1L4F100 (d) tools.

As seen in Figure 4, the wear was more severe for the 4-m cutting length machining tests, with these exhibiting more damage to the flank and the presence of well-developed wear mechanisms, such as machined material adhesion. The machined material adheres to the tool's surface overtime, promoting the development of wear mechanisms such as abrasion, coating delamination and adhesive wear. The adhesion present in the rake face of the T1L4F100 tool is presented with larger magnification in Figure 5.

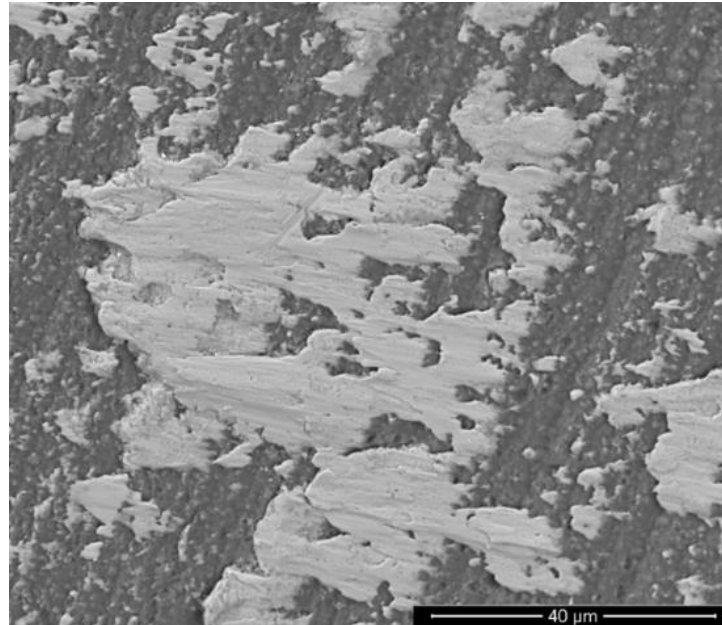


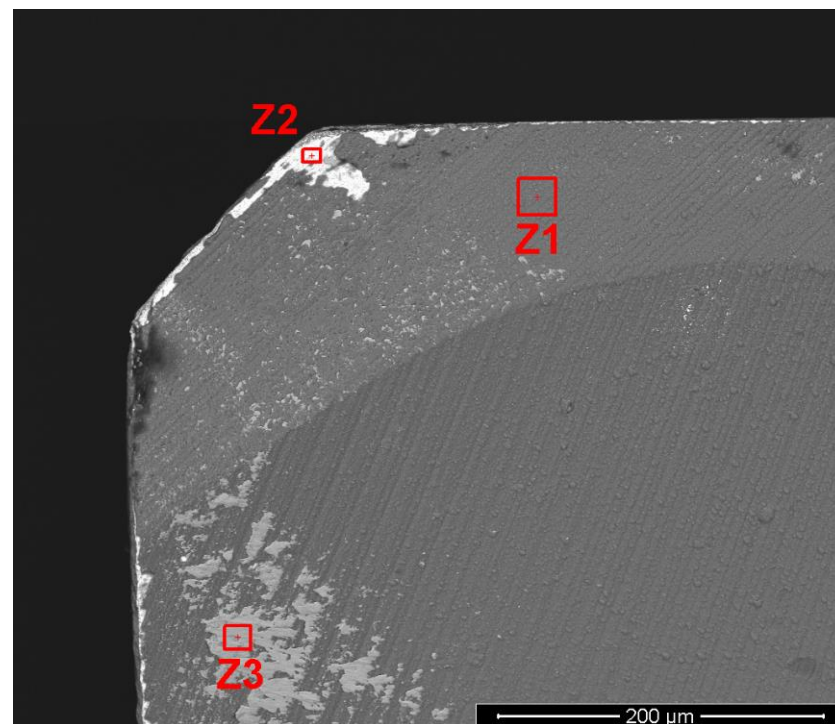
**Figure 5.** Adhered workpiece material present in the T1L4F100 tool's rake face, with a magnification of 2500 $\times$ .

The adhesive damage observed in Figure 5 was analyzed to determine if the material present on the surface was the one that was being machined. Thus, EDS analyses were performed to determine the chemical composition of the damage, as observed in Figure 6. It was indeed confirmed that the adhered material was the DSS, as its chemical composition was very close to that supplied by the manufacturer. Therefore, it can be concluded that the increase in cutting length promotes the adhesion of machined material to the tool's surface and that there is a lower amount of adhered material for the T1L2F100 condition, as seen in Figure 4c.

Regarding the influence of feed rate on the tools' wear and registered mechanisms, although there was an influence on the amount of wear that was sustained by the tools, the identified mechanisms were present in all the tested conditions, albeit in different levels of severity. In Figure 7, the tools' rake and clearance faces are depicted for the 75% and 125% feed conditions.

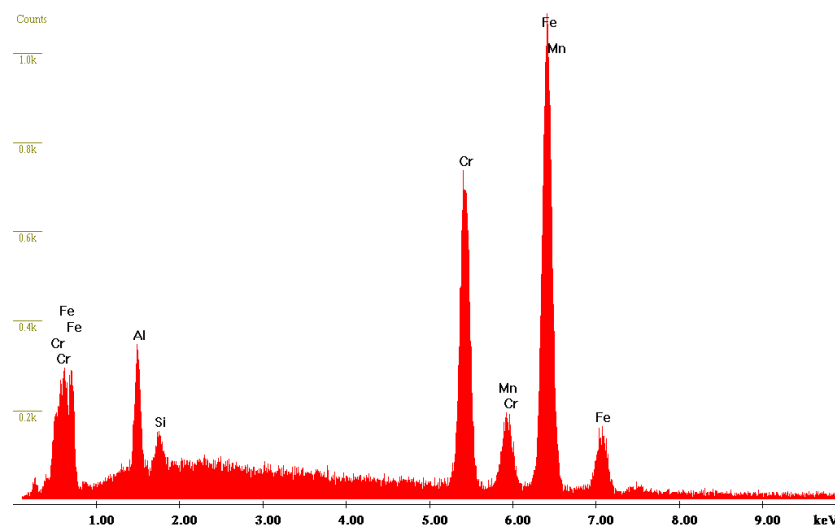
In Figure 7, it can clearly be observed that both the 75% feed rate condition and the 125% feed rate condition produced a more severe wear than that registered for the 100% feed rate (Figure 4); this was also observed in the previous section with the values of flank wear.

As previously mentioned, the main wear mechanisms that were detected during the analysis of this tool were abrasion, coating cracking, delamination and some adhesion. These are common wear mechanisms that are developed when machining DSS alloys [45,46]. Some evidence of abrasion can be observed in Figure 8.



(a)

Label A: CEMUP 15keV T1L4F100\_RF1\_003 - EDS Z3



(b)

**Figure 6.** Rake face of the T1L4F100 tool with the various zones picked for analysis (a), and analysis of zone 3 (Z3), where there are signs of adhesion (b).

As seen in Figure 8, for a test conducted at a 2-m cutting length, there were already parts of the tool's rake face with exposed substrate. There were abrasion marks, as pointed to in the picture. This was concluded to be due to the thinning of the coating in the marked area. Furthermore, there was evidence of coating spalling in the area pointed to in Figure 8. Regarding the adhered material, material adhesion was promoted by an increase in cutting length, as Figure 8 shows that the material tended to adhere to the machining grooves present in the substrate, promoting abrasive wear in that area and eventually leading to coating delamination. Some cracking in the tool's coating was also registered, especially

under the conditions of a lower feed rate, which can be observed in Figure 4. In Figure 9, this cracking process can be observed in a more detailed manner.

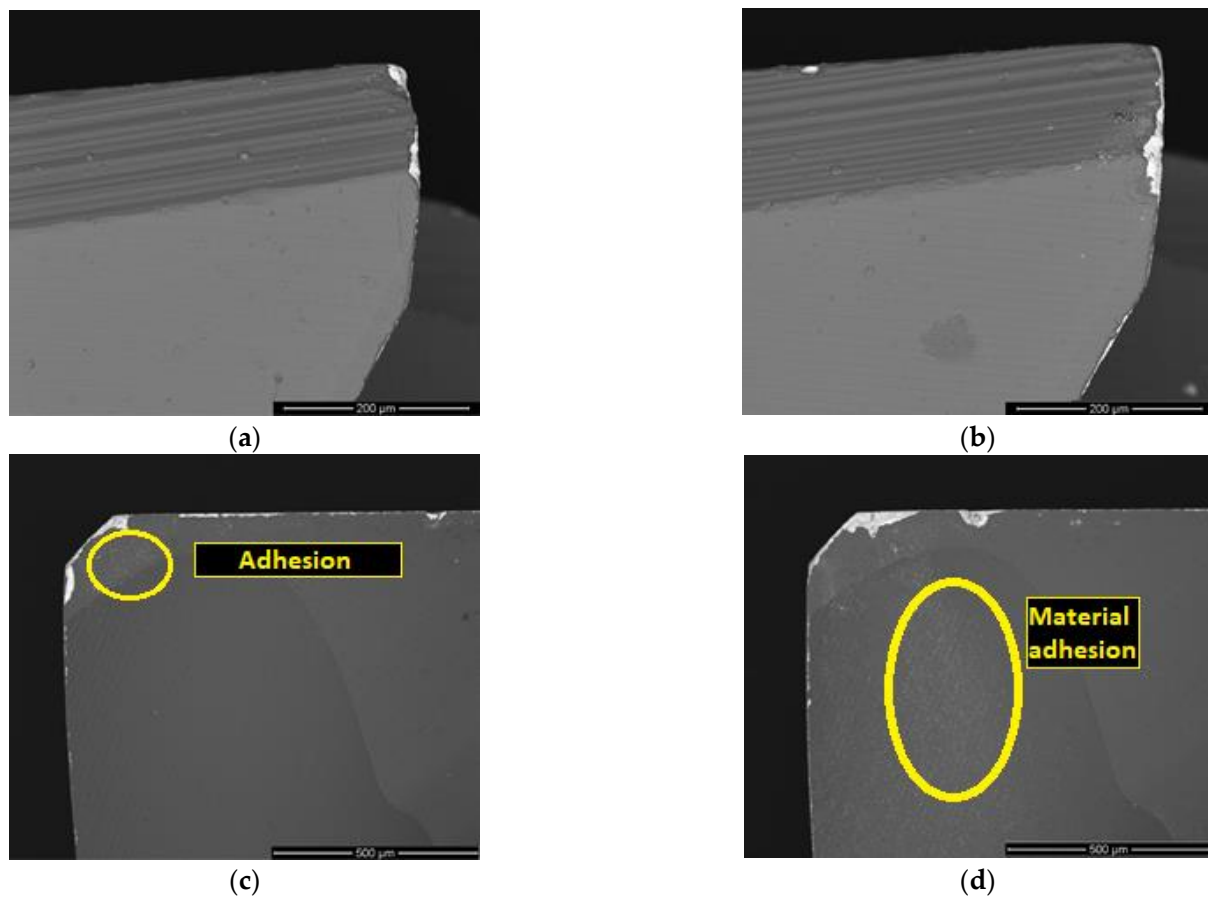


**Figure 7.** Clearance face, with a  $500\times$  magnification, of the T1L2F75 (a) and T1L2F125 (b) tools, and rake face, with a  $500\times$  magnification, of the T1L2F75 (c) and T1L2F125 (d) tools.

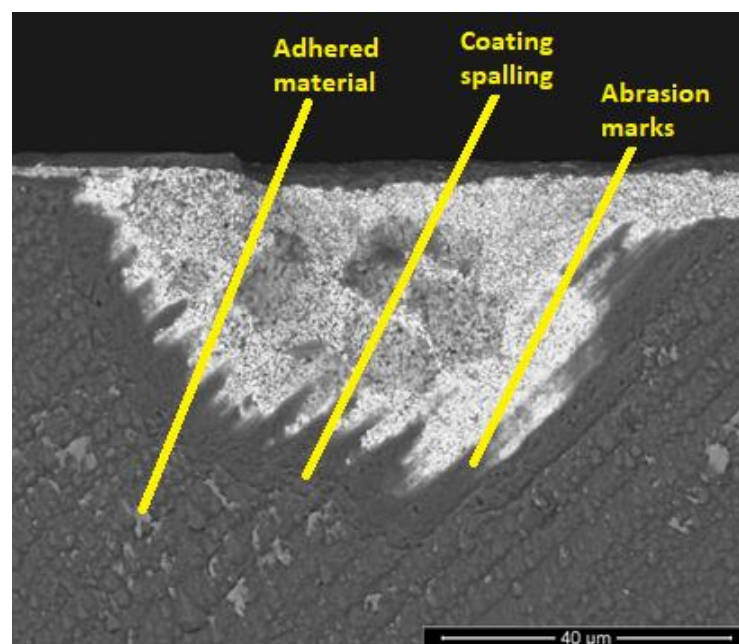


**Figure 8.** Wear mechanism analysis of the T1L2F125 rake face.

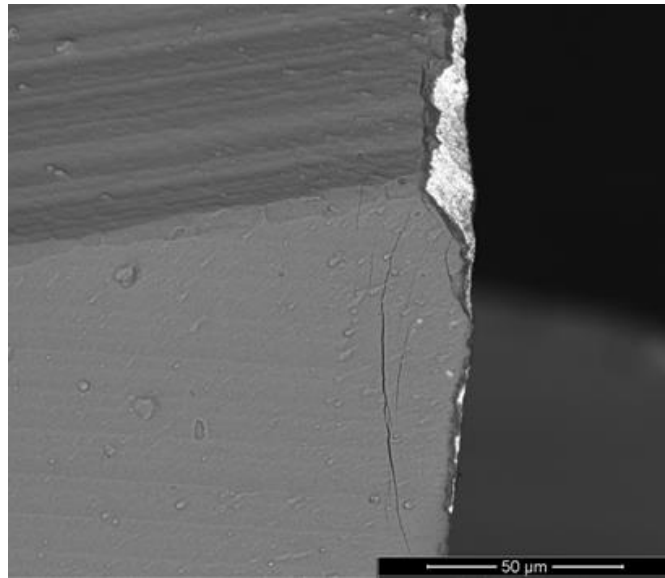


**Figure 9.** Coating cracking present on the tool's clearance face for the T1L2F75.

### 3.5.2. T2—Wear Mechanism Analysis

As observed in the case of T1, for this case the wear was also noticeable with the increase in cutting length. Regarding the wear mechanisms previously reported in the T1 tool, these were also present in T2; however, there were different severities. For example, in the case of the amount of adhered material, this was more severe in T2 than that observed in T1. The main wear mechanisms sustained by these tool types were abrasion, material adhesion, coating delamination and some coating cracking, as seen in T1, albeit at different levels.

As described in the section regarding the wear measurements performed on these tools, they exhibited more wear for longer cutting lengths; however, this wear was not as significant as recorded for the previous tools. Contrary to what was seen in T1, adhesion started to form at lower cutting lengths, as seen in Figure 10.

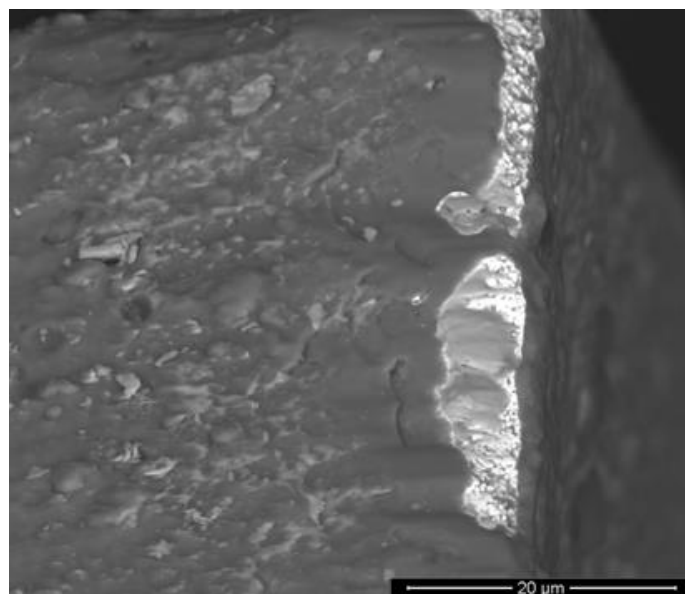


**Figure 10.** Adhered material in the T2 tool's flank, tested under the T2L2F100 condition.

This adhesion was registered in the coating's clearance and rake faces, forming primarily at lower feed rates. This adhesion to the tool's coated surface eventually leads to coating delamination by adhesive wear, as seen in Figure 11, where zones of adhered material are marked in yellow.

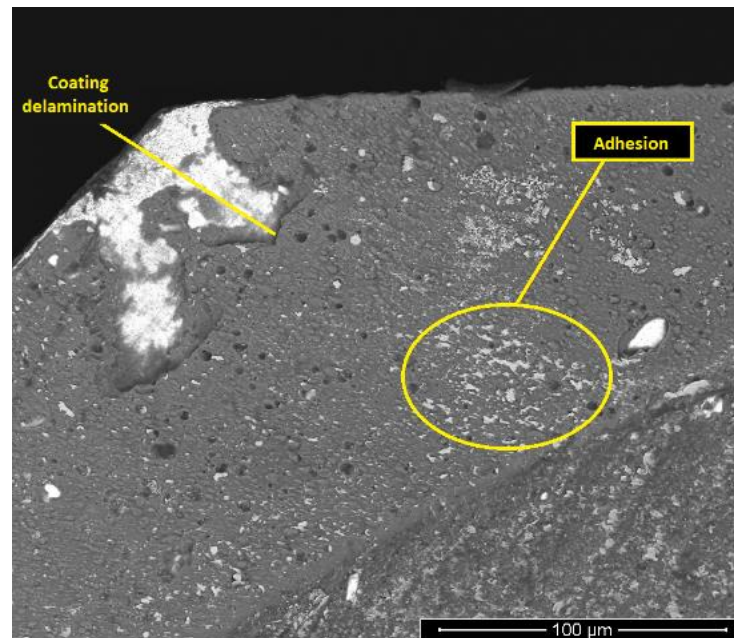


**Figure 11.** Coating delamination registered in the rake face of a T2L2F100 tool.

At higher feed rates, primarily at a 125% feed rate, the amount of adhesive wear was lower than that registered at lower feed rate values. However, the tools presented abrasion marks and cracking, exhibiting high levels of wear as well. In Figure 12, the abrasive wear can be observed in a T2 tool, tested at a 125% feed rate. The coating was abraded, exposing the substrate. However, there was some coating delamination, especially in the tool's rake face, possibly caused by adhesive wear, as shown in Figure 13.

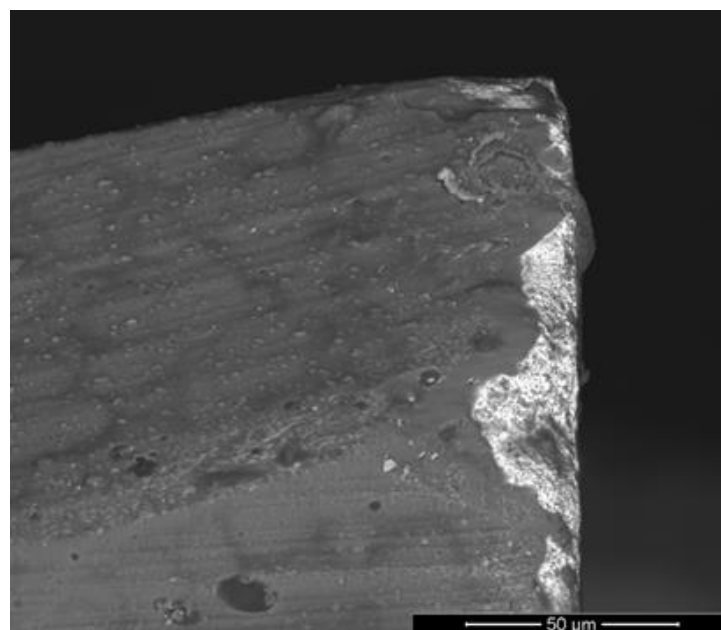


**Figure 12.** Abrasive wear on the clearance face of T2L4F125 tool.

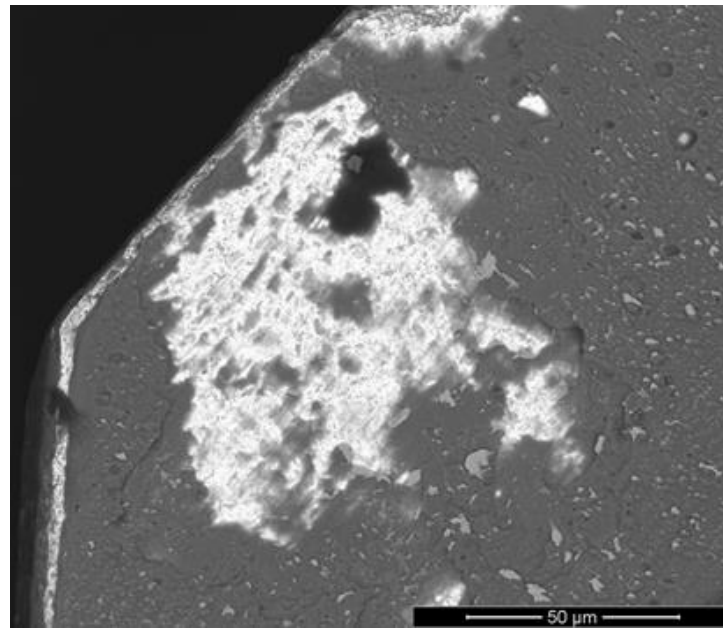


**Figure 13.** Rake face of a T2 tool tested at 4-m cutting length and 125% feed rate showing adhesive wear and coating delamination.

### 3.5.3. T3—Wear Mechanism Analysis

Regarding the wear mechanisms sustained by T3 tools, these exhibited high levels of material adhesion to the tools' surfaces, especially at high feed rates, and even originated a built-up edge. This can be observed in Figure 14.

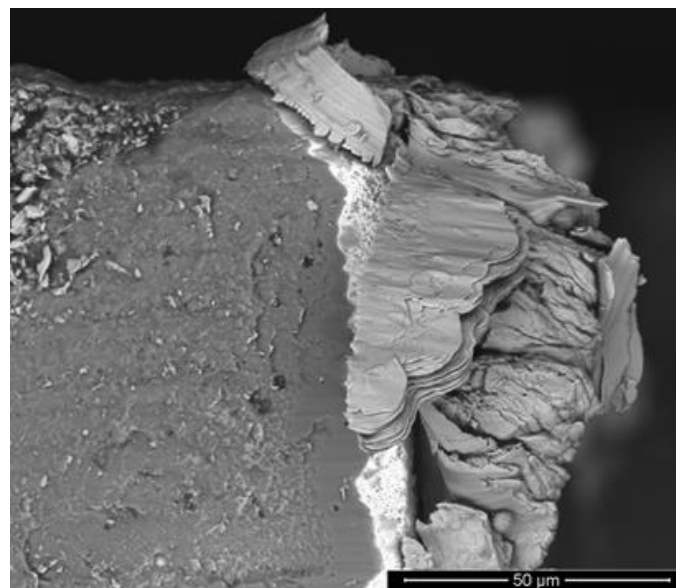


**Figure 14.** Built-up edge detected on the clearance face of a T3 tool, tested at 125% feed rate.

Other wear mechanisms were identified, being the same as the reported in the previously mentioned tools. There was evidence of abrasive wear and coating delamination, as seen in Figure 15. This delamination was promoted by the high amount of material adhesion and abrasion of the workpiece material on the tool's surface. The material adhesion promoted abrasive wear on these adhesion zones, eventually resulting in the spalling of the tool's coating (through adhesive wear).

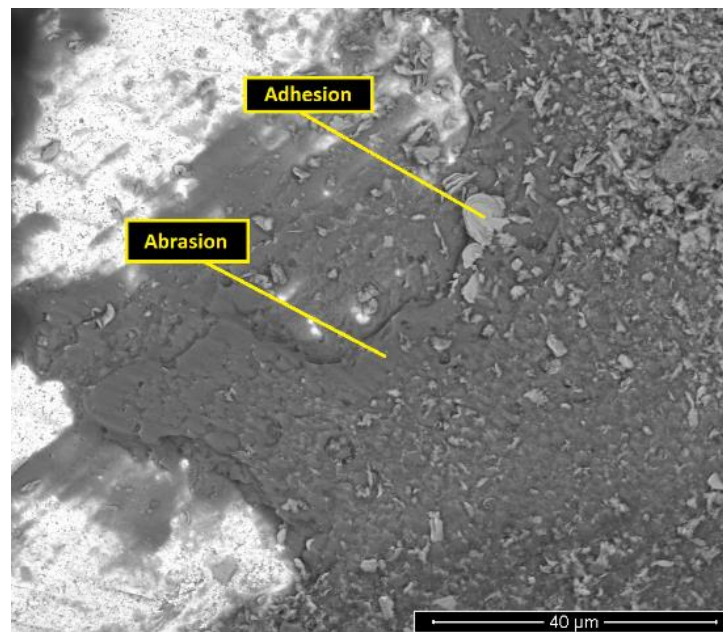


**Figure 15.** Material adhesion and abrasive wear detected on a T3 tool's rake face, tested at 125% feed rate.

Unlike in T1 and T2 tools, no major cracks were registered; however, some cracks in the nanometric scale were identified. These “nanocracks” can eventually lead to bigger ones, resulting in coating spalling and delamination. The propagation of these cracks is known to be slowed down by multi-layered coatings, such as the T3 coating in use [16,17]. This can be observed in Figure 16.

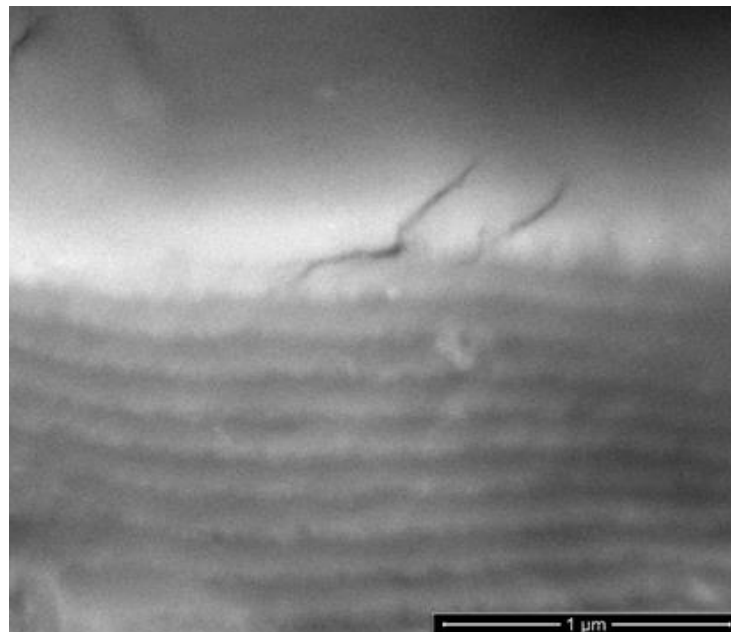


**Figure 16.** Cracks, detected in the coating of a T3 tool, tested at 75% feed rate and 4 m of cutting length.

As seen from figures presented in this subsection, this tool exhibited high amounts of adhesion and abrasion, exposing the substrate in some areas. There was, however, a low amount of flank wear reported, and this tool produced satisfactory results in terms of machined surface quality. Comparing this tool to T1, coated with the same AlCrN coating,

it can be concluded that there is a clear benefit in using a tool with four flutes to machine these types of DSS alloys.

#### 3.5.4. T4—Wear Mechanism Analysis

T4 tools exhibited the best wear performance of all the tools, exhibiting the lowest flank wear value, especially for high feed conditions. However, these tools suffered considerable damage to their rake faces. Regarding the wear mechanisms identified on these tools, all the previously mentioned were present, especially abrasive wear, coating delamination and material adhesion to the tools' surfaces. The process of coating delamination was the same as identified in the previously analyzed tools, as can be seen in Figure 17.

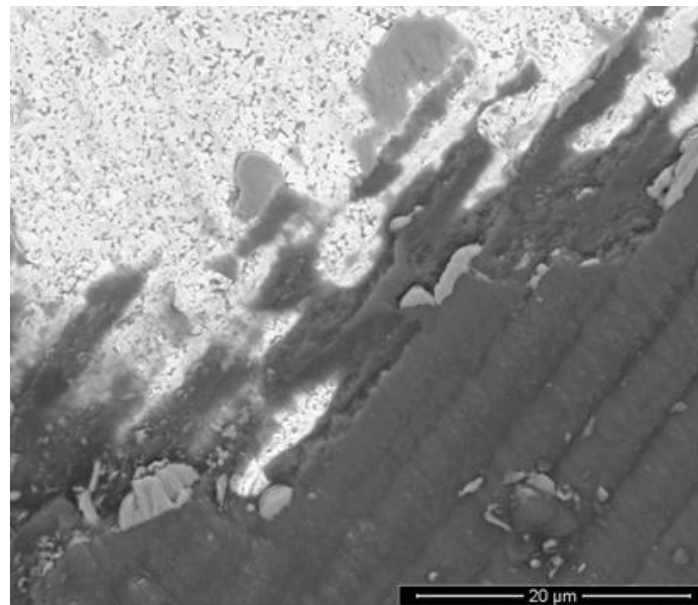


**Figure 17.** Adhesive wear detected on the T4 tool's rake face, tested at 4-m cutting length and at 100% feed rate.

The substrate's machining grooves, originated from the substrate's grinding process, promoted material adhesion on the tool's surface, thus promoting abrasion and coating delamination on these areas. This was a common trend throughout all the analyzed tools.

The wear sustained by the tools tested at 4 m of cutting length was more severe than that presented by the tools tested at 2 m, with this being a clear factor on wear mechanisms, such as adhesion, at lower feed rates. For higher feed rates, adhesion was identified, but in a smaller amount than that registered at lower feed rates. There was clear evidence of abrasion being the dominant wear mechanism for this tool at a 125% feed rate. Evidence of abrasion at a high feed rate can be observed in Figure 18.

There was no evidence of cracks detected in the analysis of this coating; also, it exhibited the least amount of flank wear for higher and lower feed rates. However, these tools sustained some wear on the rake faces, which can be attributed to chip formation and removal, and the material adhering to the rake faces being pushed upward, promoting adhesion to the tools' surfaces. As seen in all the previously presented tools, this adhesion promoted the delamination of the coating, resulting in the high wear of the rake faces.

#### 3.6. Summary of the Analyses' Results

In the present subsection, the summary of all the conducted analyses is performed. A comparison of the results obtained for the produced surface roughness, flank wear and registered wear mechanisms is made.

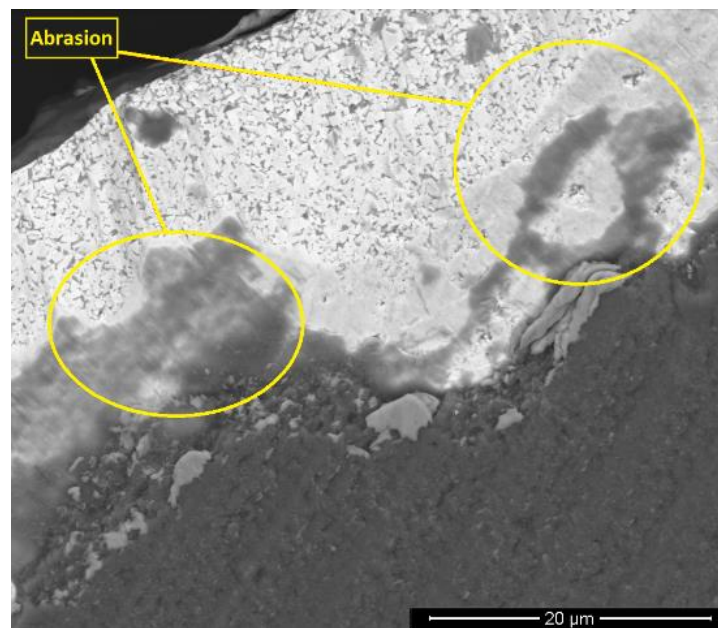


**Figure 18.** Abrasion marks detected on T4 tool's rake face, tested at 125% feed rate.

### 3.6.1. Surface Roughness Analysis Summary

In this section, the various measurements made using all the tool types in all the test conditions are presented. Both the Ra measurements taken in the radial and tangential directions are presented in Figures 19 and 20, and the test conditions are presented as seen in Section 2. The number after “L” indicates the cutting length used in that test, and the number that follows “F” indicates the percentage of feed rate that was used in the machining test.

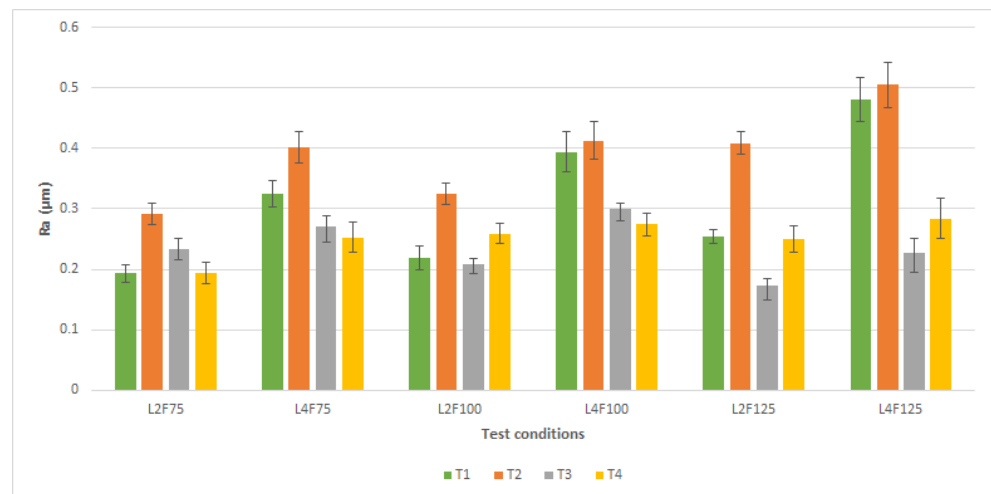


**Figure 19.** Average values of Ra, measured in the radial direction, produced by T1, T2, T3 and T4 tools for all the different test conditions.

As previously noticed in the subsections dedicated to the individual tool analysis, the surface roughness tended to increase with the increase in cutting length; this was expected, as the tool wear is more intense for higher values of cutting length. This was verified in all the tested tools, and there was also a variation in surface roughness with feed variation, as this parameter is known to have high influence on the surface roughness [14,15]. Regarding the variation in surface roughness with feed rate, the predominant trend was that lower feed rates will confer a better surface finish to the machined part, except for T3, where an

increase in feed rate produced a better surface quality than at lower values of feed rate. It is worthy to note, however, that the surface roughness values produced by T3 were the best, being closely followed by T4. In fact, the surface quality produced at the 125% feed rate by the T3 and T4 tools was on par with the surface roughness quality produced by the T1 and T2 at the 75% feed rate, indicating that the four-fluted AlCrN-coated end-mill and the four-fluted TiAlSiN-coated end-mill are good choices for the conduction of finishing operations in this kind of material. The number of flutes has a great influence in the machining of this material, especially regarding the AlCrN-coated tools, as it can be observed that the two flutes' tools produced a worse surface quality than that of the four-fluted AlCrN-coated tool [44]. In Figure 21, the variation of machined surface quality for different feed rate values can be observed for the 2-m and 4-m cutting lengths (in the radial direction, as the identified trends were the same for both directions and the values were similar). It was observed that the trends were common for both 2 and 4 m of cutting length; however, the T4 tools seemed to be the least affected by the increase in cutting length, with the roughness values not increasing drastically for higher cutting length values, especially when compared to T1 and T2 tools. The T3 tools were also resistant to this variation. Furthermore, the results obtained for lower feed rate values were higher than those registered for T4.

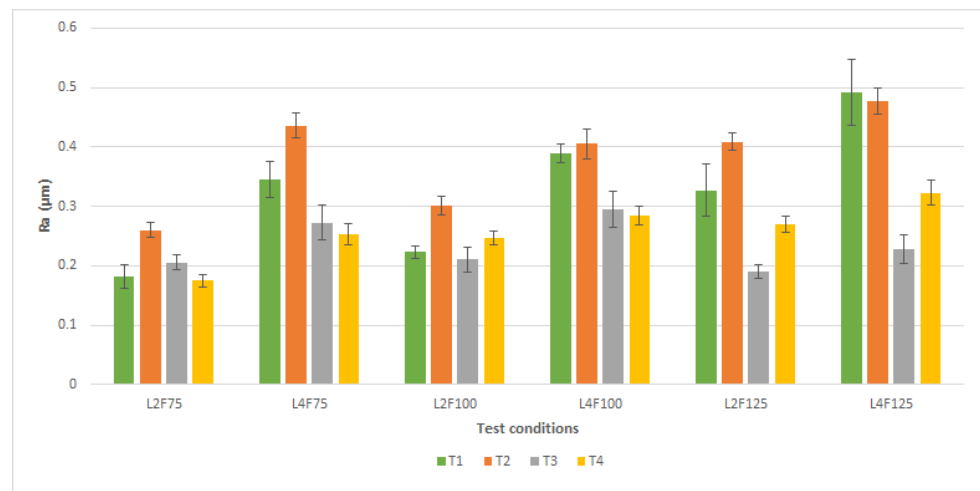
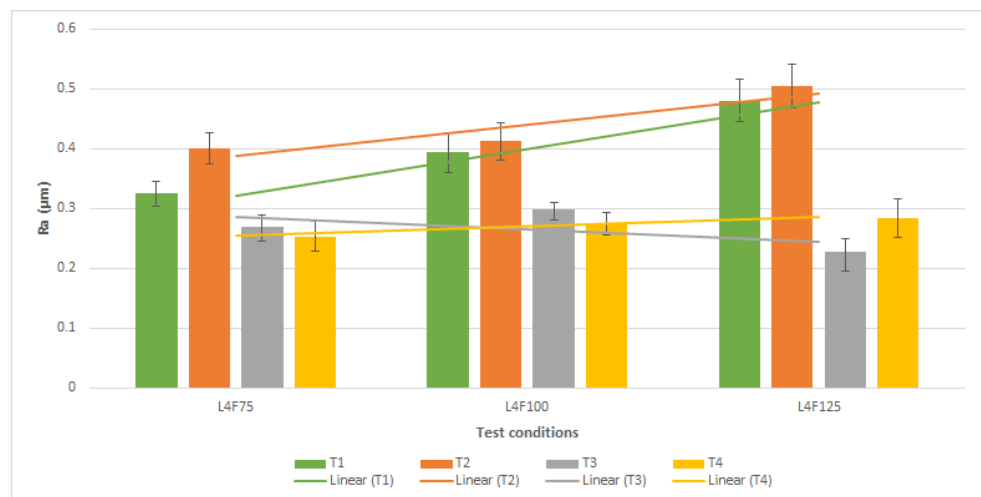


**Figure 20.** Average values of Ra, measured in the tangential direction, produced by T1, T2, T3 and T4 tools for all the different test conditions.

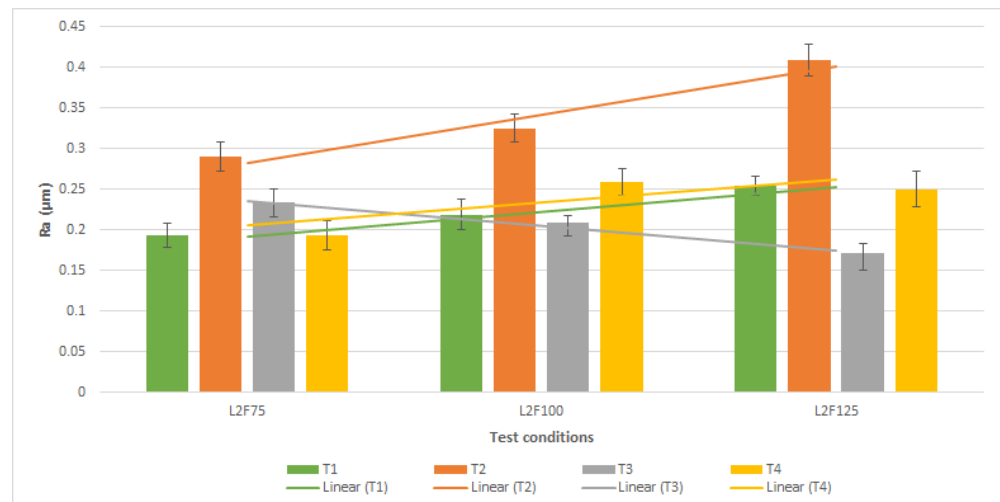
It is worthy to note that the amount of registered tool wear negatively impacts the machined surface quality, with the conditions that produced the highest amount of wear producing the worst machined surface quality [14,15]. Tools that exhibited higher levels of VB tended to produce a worse machined surface quality, primarily since the substrate was exposed (adhesive wear and coating delamination/spalling), and were subject to wear mechanisms such as abrasive wear. This altered the cutting edge's geometry, inducing this higher surface roughness value. However, as previously mentioned, the machining parameters highly impacted the machined surface quality, with the T3 tool being a prime example of this fact.

### 3.6.2. Flank Wear Measurement Summary

In the present subsection, all the calculated average values of flank wear, measured on the clearance faces of all the tested tools, are discussed. As seen in the section regarding surface roughness analysis, all the collected values are presented in graphical form in Figures 22 and 23.



(a)



(b)

**Figure 21.** Average values of Ra, measured in the radial direction for T1, T2, T3 and T4 tools, for the test conditions conducted at 2-m cutting length (a); and 4-m cutting length (b).

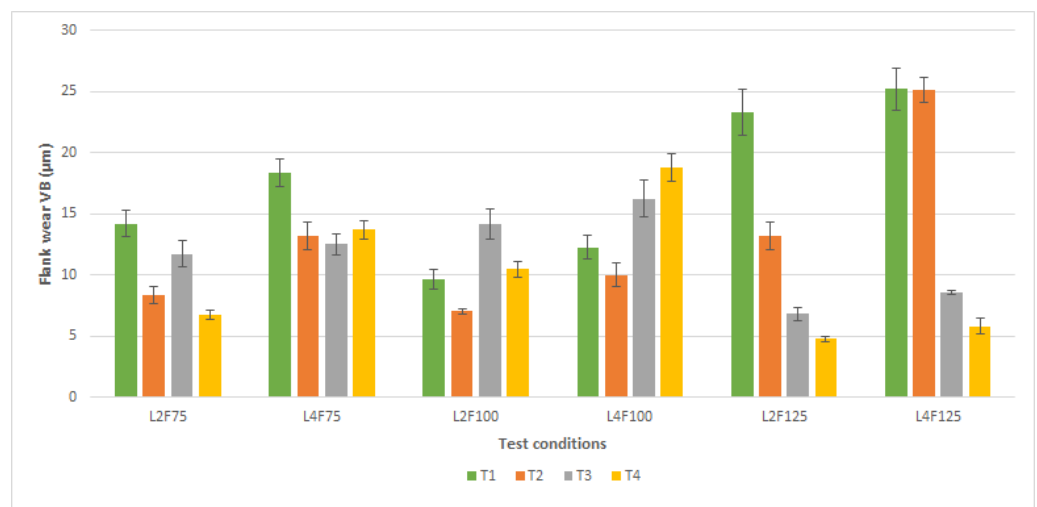


**Figure 22.** Average values of VB, measured on the clearance faces of the T1, T2, T3 and T4 tools, for all the different test conditions.

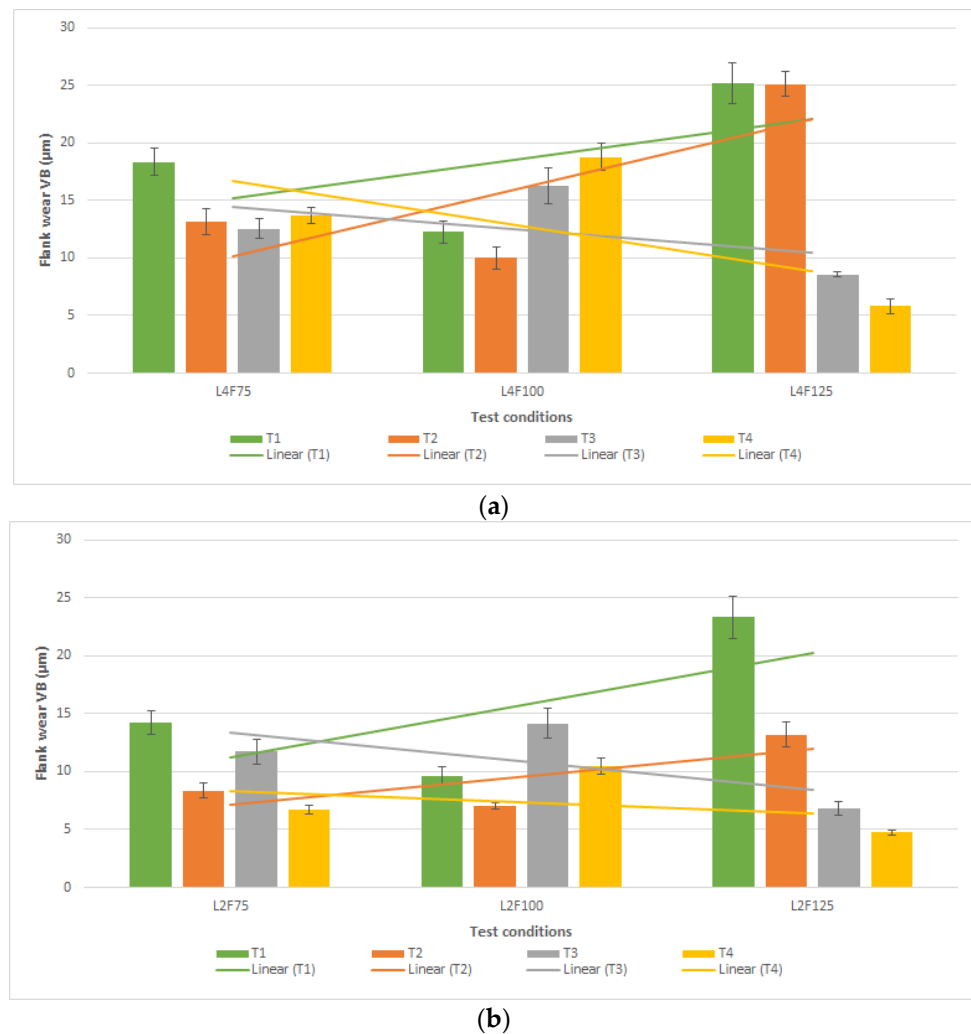


**Figure 23.** Average values of VB, measured on the clearance faces of the T1, T2, T3 and T4 tools, for the test conditions conducted at 2-m cutting length (a); and 4-m cutting length (b).

In Figures 22 and 23, a clear increase in wear with an increase in cutting length and feed rate was clearly observed for T1 and T2 tools. Furthermore, T1 tools seemed to be the most affected, in terms of wear, by feed rate variation (positive or negative), whereas T2 seemed to be the most affected by the variation in cutting length, especially at higher feed rate values. Regarding tools T3 and T4, these showed the most wear of all tools for the original feed rate conditions, with T3 being slightly affected by cutting length variation, and T4 being significantly more affected by the variation of this parameter at a 100% feed rate. However, T3 and T4 tools produced low wear for the lower feed rate values, producing, as well, the lowest amount of flank wear registered for the high feed rate test conditions. In fact, the wear presented by these tools was minimal for these test conditions, indicating that in terms of wear behavior these would be more suited for the machining of this material, especially at high feed values. Regarding once again tools T1 and T2, although these produced the best behavior at the original feed rate, and T2 even registered the second lowest values for flank wear tested under the condition of a 2-m cutting length and 75% feed rate, these tools exhibited high wear under the conditions of a 4-m cutting length and under the test conditions of a higher feed rate (125%), meaning that the original parameters were the most suited for machining with these tool types. It is shown that T1 was more sensitive to feed rate variations, whereas T2 was more sensitive to cutting length variations, in terms of flank wear.

### 3.6.3. Wear Mechanism Analysis Summary

The wear mechanisms that were observed in the tools, mainly abrasive and adhesive wear, are expected when machining DSS alloys [46,47]. It is worthy to note that the tool type that suffered the least amount of adhesive wear was T1, since this tool only has two flutes. This enables a better chip evacuation, as the lubricant can cool and clean a larger area. However, in this tool there was evidence of abrasion, coating delamination and cracking, despite the AlCrN coating's structure. This is due to, once again, the tool having only two flutes. Thus, a four-fluted or plus design is preferred to machine this type of material.

T3 tools exhibited high amounts of adhesion when compared to the other tools, especially at higher cutting lengths. This led to the formation of a built-up edge. However, the flank wear that was registered for these tools was not very severe. The tools coated with TiAlSiN showed the best wear performance. Indeed, this coating is well known to perform well in terms of wear, even in the machining of hard materials [56]. Although these tools exhibited the same wear patterns as the other tools, these were not so severe in the flank. However, these tools suffered damage on their rake faces, due to the buildup of adhered material in this area. In Table 16, the summary of the wear analysis performed on all tested tools is presented, showing the main mechanisms registered for these.

**Table 16.** Summary of the SEM wear analysis for each of the tested tools, mentioning the main wear type and mechanism identified.

Tool	SEM Wear Analysis Summary
T1	- Abrasive wear; - Coating delamination; - Coating cracking; - Material adhesion.
T2	- Material adhesion; - Abrasive wear; - Adhesive wear; - Coating delamination; - Coating cracking.
T3	- Material adhesion; - Adhesive wear; - Built-up edge; - Abrasive wear; - Coating delamination.
T4	- Abrasive wear; - Material adhesion; - Adhesive wear; - Coating delamination.

## 4. Conclusions

In the present work, an analysis of the wear behavior of four milling tools used in machining operations of DSS was presented. Four tools with different geometries and coatings were evaluated. One tool had two flutes (T1) and three tools had four flutes (T2, T3 and T4). The tested coatings were TiAlN (T2), AlCrN (T1 and T3) and TiAlSiN (T4). Additionally, the influence of cutting length and feed rate was evaluated based on the tools' wear and production quality (machined surface quality). Furthermore, the wear of the tested tools was analyzed, and the present wear mechanisms identified.

Regarding the tested tools' performance, it was found that T1 (two-flute, AlCrN) and T2 (TiAlN) tools were not the most suited to machine this DSS alloy, as they presented severe wear for the highest feed rate conditions. Their flank wear was heavily promoted by an increase in cutting length. This can be related to the coating's properties in the case of T2, as this coating did not present the best mechanical properties (of all evaluated coatings). However, in the case of T1, the increased wear and lack of performance can be attributed

to the fact that this tool only had two cutting edges. The AlCrN coating's properties were quite good, presenting high values of  $H/E$  (0.11) and  $H^3/E^2$  (0.395) (when compared to the other analyzed coatings) [53,54], which are representative of a good coating wear behavior. However, the AlCrN-coated tools presented a high  $E_c/E_s$  ratio value (0.581, the highest of all analyzed coatings), indicating that it is quite prone to phenomena such as coating cracking and delamination [55].

As for the performances of T3 (four-fluted, AlCrN) and T4 (TiAlSiN), these tools exhibited the best performances, with the T3 tool producing the best results in terms of machined surface quality (for highest feed rate values). However, this tool presented more wear when compared to T4. Furthermore, for the rest of the test conditions (75% and 100% feed rate value), the T4 tool produced the best machined surface quality. As for flank wear, the T4 tool clearly outperformed the rest of the tested tools. This can be attributed to, not only the four-fluted geometry, but also to the mechanical properties of the TiAlSiN coating, which presented a high value of  $H/E$  (0.081, which is very close to 0.1) and a high  $H^3/E^2$  value (0.142; these ratios' values were the second highest of all the analyzed coatings, being very close to the AlCrN coatings), and a lower  $E_c/E_s$  ratio value (0.435), when compared to the AlCrN coating (in fact, this value was the lowest for all the analyzed substrate/coating systems).

Regarding the identified wear mechanisms, these were common among all evaluated tools, albeit at different levels of severity. These were: abrasive wear, adhesive wear and coating delamination/spalling. The coating failure method seemed to be common to all tools, as the workpiece material adheres to the machining grooves left by the substrate's grinding process. This adhesion promotes abrasive wear and further material buildup in these areas, eventually resulting in the spalling of the tool coating.

**Author Contributions:** V.F.C.S.: investigation, formal analysis and writing—original draft; F.J.G.S.: conceptualization, methodology, project administration, resources, supervision and writing—review and editing; R.A.: coating development, formal analysis, resources and visualization; G.P.: formal analysis, validation and writing—review and editing; A.B.: formal analysis, validation and writing—review and editing; J.S.F.: investigation and supervision. All authors have read and agreed to the published version of the manuscript.

**Funding:** The present work was conducted and funded under the scope of the project ON-SURF (ANI | P2020 | POCI-01-0247-FEDER-024521, co-funded by Portugal 2020 and FEDER, through the COMPETE 2020-Operational Programme for Competitiveness and Internationalisation.

**Data Availability Statement:** No data is made available regarding this work.

**Acknowledgments:** F.J.G. Silva thanks INEGI—Instituto de Ciência e Inovação em Engenharia Mecânica e Engenharia Indústria for its support. The authors would like to thank Rui Rocha from CEMUP (Porto, Portugal), due to his active collaboration in getting the best SEM pictures and helping with his critical analysis of some phenomena. The authors also would like to thank Ing. Ricardo Alexandre for his extremely important role in providing all the coatings through the TEandM company, and Eng. Nuno André for providing the substrate material and uncoated tools through the Inovatools company.

**Conflicts of Interest:** The authors declare no conflict of interest.

## References

1. Cheng, X.; Wang, Y.; Li, X.; Dong, C. Interaction between austenite-ferrite phases on passive performance of 2205 duplex stainless steel. *J. Mater. Sci. Technol.* **2018**, *34*, 2140–2148. [[CrossRef](#)]
2. Jebaraj, A.V.; Ajaykumar, L.; Deepak, C.R.; Aditya, K.V.V. Weldability, machinability and surfacing of commercial duplex stainless steel AISI2205 for marine applications—A recent review. *J. Adv. Res.* **2017**, *8*, 183–199. [[CrossRef](#)] [[PubMed](#)]
3. Nomani, J.; Pramanik, A.; Hilditch, T.; Littlefair, G. Chip formation mechanism and machinability of wrought duplex stainless steel alloys. *Int. J. Adv. Technol.* **2015**, *80*, 1127–1135. [[CrossRef](#)]
4. Chail, G.; Kangas, P. Super and hyper duplex stainless steels: Structures, properties, and applications. *Procedia Struct. Integr.* **2016**, *2*, 1755–1762. [[CrossRef](#)]
5. Nomani, J.; Pramanik, A.; Hilditch, T.; Littlefair, G. Machinability study of first generation duplex (2205), second generation duplex (2507) and austenite stainless steel during drilling process. *Wear* **2013**, *304*, 20–28. [[CrossRef](#)]

6. Koyee, R.D.; Heisel, U.; Eisseler, R.; Schmauder, S. Modeling and optimization of turning duplex stainless steels. *J. Manuf. Processes* **2014**, *16*, 451–467. [[CrossRef](#)]
7. Gowthaman, P.S.; Jeyakumar, S.; Saravanan, B.A. Machinability and tool wear mechanism of Duplex stainless steel—A review. *Mater. Today Proc.* **2020**, *26*, 1423–1429. [[CrossRef](#)]
8. Sahithi, V.V.D.; Malayadrib, T.; Srilatha, N. Optimization of Turning Parameters on Surface Roughness Based on Taguchi Technique. *Mater. Today Proc.* **2019**, *18*, 3657–3666. [[CrossRef](#)]
9. Thhabadira, I.; Daniyan, I.A.; Masu, L.; Van Staden, L.R. Process Design and Optimization of Surface Roughness during M200 TS Milling Process using the Taguchi Method. *Procedia CIRP* **2019**, *84*, 868–873. [[CrossRef](#)]
10. Vardhan, M.V.; Sankaraiah, G.; Johan, M.; Rao, H.J. Optimization of Parameters in CNC milling of P20 steel using Response Surface methodology and Taguchi Method. *Mater. Today Proc.* **2017**, *4*, 9163–9169. [[CrossRef](#)]
11. Zhang, J.Z.; Chen, J.C.; Kirby, E.D. Surface roughness optimization in an end-milling operation using the Taguchi design method. *J. Mater. Process. Technol.* **2007**, *184*, 233–239. [[CrossRef](#)]
12. Kumar, S.; Saravanan, I.; Patnaik, L. Optimization of surface roughness and material removal rate in milling of AISI 1005 carbon steel using Taguchi approach. *Mater. Today Proc.* **2019**, *22*, 654–658. [[CrossRef](#)]
13. Selvaraj, D.P. Optimization of cutting force of duplex stainless steel in dry milling operation. *Mater. Today Proc.* **2017**, *4*, 11141–11147. [[CrossRef](#)]
14. Airao, J.; Chaudhary, B.; Bajpai, V.; Khanna, N. An Experimental Study of Surface Roughness Variation in End Milling of Super Duplex 2507 Stainless Steel. *Mater. Today Proc.* **2018**, *5*, 3682–3689. [[CrossRef](#)]
15. Policena, M.R.; Devitte, C.; Fronza, G.; Garcia, R.F.; Souza, A.J. Surface roughness analysis in finishing end-milling of duplex stainless steel UNS S32205. *Inter. J. Adv. Manuf. Technol.* **2018**, *98*, 1617–1625. [[CrossRef](#)]
16. Sousa, V.F.C.; Silva, F.J.G. Recent Advances in Turning Processes Using Coated Tools—A Comprehensive Review. *Metals* **2020**, *10*, 170. [[CrossRef](#)]
17. Sousa, V.F.C.; Silva, F.J.G. Recent Advances on Coated Milling Tool Technology—A Comprehensive Review. *Coatings* **2020**, *10*, 235. [[CrossRef](#)]
18. Martinho, R.P.; Silva, F.J.G.; Baptista, A.P.M. Cutting forces and wear analysis of Si<sub>3</sub>N<sub>4</sub> diamond coated tools in high speed machining. *Vacuum* **2008**, *82*, 1415–1420. [[CrossRef](#)]
19. Paiva, J.M.F.; Amorim, F.L.; Soares, P.C.; Veldhuis, S.C.; Mendes, L.A.; Torres, R.D. Tribological behavior of superduplex stainless steels against PVD hard coatings on cemented carbide. *Inter. J. Adv. Manuf. Technol.* **2019**, *90*, 1649–1658. [[CrossRef](#)]
20. Silva, F.J.G.; Martinho, R.; Andrade, M.; Baptista, A.P.M.; Alexandre, R. Improving the Wear Resistance of Moulds for the Injection of Glass Fibre-Reinforced Plastics Using PVD Coatings: A Comparative Study. *Coatings* **2017**, *7*, 28. [[CrossRef](#)]
21. Silva, F.J.G.; Martinho, R.P.; Alexandre, R.J.D.; Baptista, A.P.M. Increasing the wear resistance of molds for injection of glass fiber reinforced plastics. *Wear* **2011**, *271*, 2494–2499. [[CrossRef](#)]
22. Silva, F.J.G.; Martinho, R.P.; Baptista, A.P.M. Characterization of laboratory and industrial CrN/CrCn/Diamond-like carbon coatings. *Thin Solid Films* **2014**, *550*, 278–284. [[CrossRef](#)]
23. Silva, F.J.G.; Fernandes, A.J.S.; Costa, F.M.; Teixeira, V.; Baptista, A.P.M.; Pereira, E. Tribological behaviour of CVD diamond films on steel substrates. *Wear* **2003**, *255*, 846–853. [[CrossRef](#)]
24. Silva, F.J.G.; Fernandes, A.J.S.; Costa, F.M.; Baptista, A.P.M.; Pereira, E. Unstressed PACVD diamond films on steel pre-coated with a composite multilayer. *Surf. Coat. Technol.* **2005**, *191*, 102–107. [[CrossRef](#)]
25. Baptista, A.; Silva, F.J.G.; Porteiro, J.; Míguez, J.L.; Pinto, G. Sputtering physical vapour deposition (PVD) coatings: A critical review on process improvement and market trend demands. *Coatings* **2018**, *8*, 402. [[CrossRef](#)]
26. Baptista, A.; Silva, F.J.G.; Porteiro, J.; Míguez, J.L.; Pinto, G.; Fernandes, L. On the Physical Vapour Deposition (PVD): Evolution of Magnetron Sputtering Processes for Industrial Applications. *Procedia Manuf.* **2018**, *17*, 746–757. [[CrossRef](#)]
27. Martinho, R.P.; Silva, F.J.G.; Martins, C.; Lopes, H. Comparative study of PVD and CVD cutting tools performance in milling of duplex stainless steel. *Int. J. Adv. Manuf. Technol.* **2019**, *102*, 2423–2439. [[CrossRef](#)]
28. Ginting, A.; Skein, R.; Cuaca, D.; Herdianto, P.; Masyithah, Z. The characteristics of CVD- and PVD-coated carbide tools in hard turning of AISI 4340. *Measurement* **2018**, *129*, 548–557. [[CrossRef](#)]
29. Koseki, S.; Inoue, K.; Morito, S.; Ohba, T.; Usuki, H. Comparison of TiN-coated tools using CVD and PVD processes during continuous cutting of Ni-based superalloys. *Surf. Coat. Technol.* **2015**, *283*, 353–363. [[CrossRef](#)]
30. Caliskan, H.; Panjan, P.; Kurbanoglu, C. 3.16 Hard coatings on cutting tools and surface finish. *Compr. Mater. Finish.* **2017**, 230–242.
31. Paiva, J.M.F.; Torres, R.D.; Amorim, F.L.; Covelli, D.; Tauhiduzzaman, M.; Veldhuis, S.; Dosbaeva, G.; Fox-Rabinovich, G. Frictional and wear performance of hard coatings during machining of superduplex stainless steel. *Int. J. Adv. Manuf. Technol.* **2017**, *92*, 423–432. [[CrossRef](#)]
32. Klocke, F.; Krieg, T. Coated tools for metal cutting—Features and applications. *CIRP Ann.* **1999**, *48*, 515–525. [[CrossRef](#)]
33. Fernández-Abia, A.I.; Barreiro, J.; Fernández-Larrinoa, J.; de Lacalle, L.N.L.; Fernández-Valdivielso, A.; Pereira, O.M. Behaviour of PVD Coatings in the Turning of Austenitic Stainless Steels. *Procedia Eng.* **2013**, *63*, 133–141. [[CrossRef](#)]
34. Vasu, M.; Nayaka, H.S. Investigation of Cutting Force Tool Tip Temperature and Surface Roughness during Dry Machining of Spring Steel. *Mater. Today Proc.* **2018**, *5*, 7141–7149. [[CrossRef](#)]
35. Phokobye, S.N.; Daniyan, I.A.; Thhabadira, I.; Masu, L.; Van Staden, L.R. Model Design and Optimization of Carbide Milling Cutter for Milling Operation of M200 Tool Steel. *Procedia CIRP* **2019**, *84*, 954–959. [[CrossRef](#)]

36. Strafford, K.N.; Audy, J. Indirect monitoring of machinability in carbon steels by measurement of cutting forces. *J. Mater. Process. Technol.* **1997**, *67*, 150–156. [[CrossRef](#)]
37. Venkatesan, K.; Manivannan, K.; Devendiran, S.; Mathew, A.T.; Ghazaly, N.M.; Aadhavan; Benny, S.M.N. Study of Forces, Surface Finish and Chip Morphology on Machining of Inconel 825. *Procedia Manuf.* **2019**, *30*, 611–618. [[CrossRef](#)]
38. Caudill, J.; Schoop, J.; Jawahir, I.S. Numerical Modeling of Cutting Forces and Temperature Distribution in High Speed Cryogenic and Flood-cooled Milling of Ti-6Al-4V. *Procedia CIRP* **2019**, *82*, 83–88. [[CrossRef](#)]
39. Fernández-Abia, A.I.; Barreiro, J.; de Lacalle, L.N.L. Behavior of austenitic stainless steels at high speed turning using specific force coefficients. *Int. J. Adv. Manuf. Technol.* **2012**, *62*, 505–515. [[CrossRef](#)]
40. Batuev, V.A.; Batuev, V.V.; Ardashev, D.V.; Shipulin, L.V.; Degtyareva-Kashutina, A.S. Analytical Calculation of Cutting Forces and Analysis of their Change at 3-D Milling. *Procedia Manuf.* **2019**, *32*, 42–49. [[CrossRef](#)]
41. Davoudinejad, A.; Chiappini, E.; Tirelli, S.; Annoni, M.; Strano, M. Finite Element Simulation and Validation of Chip Formation and Cutting Forces in Dry and Cryogenic Cutting of Ti-6Al-4V. *Procedia Manuf.* **2015**, *1*, 728–739. [[CrossRef](#)]
42. Bhopale, S.; Jagatap, K.R.; Lamdhade, G.K.; Darade, P.D. Cutting Forces during Orthogonal Machining Process of AISI 1018 Steel: Numerical and Experimental Modeling. *Mater. Today Proc.* **2017**, *4*, 8454–8462. [[CrossRef](#)]
43. Mebrahitom, A.; Choon, W.; Azhari, A. Side Milling Machining Simulation Using Finite Element Analysis: Prediction of Cutting Forces. *Mater. Today Proc.* **2017**, *4*, 5215–5221. [[CrossRef](#)]
44. Gouveia, R.; Silva, F.J.G.; Reis, P.; Baptista, A.P.M. Machining duplex stainless steel: Comparative study regarding end mill coated tools. *Coatings* **2016**, *6*, 51. [[CrossRef](#)]
45. Ahmed, Y.S.; Paiva, J.; Covelli, D.; Veldhuis, S. Investigation of Coated Cutting Tool Performance during Machining of Super Duplex Stainless Steels through 3D Wear Evaluations. *Coatings* **2017**, *7*, 127. [[CrossRef](#)]
46. Dos Santos, A.G.; da Silva, M.B.; Jackson, M.J. Tungsten carbide micro-tool wear when micro milling UNS S32205 duplex stainless steel. *Wear* **2018**, *414–415*, 109–117. [[CrossRef](#)]
47. Diniz, A.E.; Machado, A.R.; Corrêa, J.G. Tool wear mechanisms in the machining of steels and stainless steels. *Int. J. Adv. Manuf. Technol.* **2016**, *87*, 3157–3168. [[CrossRef](#)]
48. Silva, F.; Martinho, R.; Martins, C.; Lopes, H.; Gouveia, R. Machining GX2CrNiMoN26-7-4 DSS Alloy: Wear Analysis of TiAlN and TiCN/Al<sub>2</sub>O<sub>3</sub>/TiN Coated Carbide Tools Behavior in Rough End Milling Operations. *Coatings* **2019**, *9*, 392. [[CrossRef](#)]
49. Krolczyk, G.M.; Nieslony, P.; Legutko, S. Determination of tool life and research wear during duplex stainless steel turning. *Arch. Civ. Mech. Eng.* **2015**, *15*, 347–354. [[CrossRef](#)]
50. Rajaguru, J.; Arunachalam, N. Coated tool Performance in Dry Turning of Super Duplex Stainless Steel. *Procedia Manuf.* **2017**, *10*, 601–611. [[CrossRef](#)]
51. Suárez, A.; de Lacalle, L.N.L.; Polvorosa, R.; Veiga, F.; Wretland, A. Effects of high-pressure cooling on the wear patterns on turning inserts used on alloy IN718. *Mater. Manuf. Process.* **2017**, *32*, 678–686. [[CrossRef](#)]
52. ISO 8688-2:1986; Tool Life Testing in Milling—Part 2: End Milling. International Organization for Standardization: Geneva, Switzerland, 1986.
53. Leyland, A.; Matthews, A. On the significance of the H/E ratio in wear control: A nanocomposite coating approach to optimised tribological behaviour. *Wear* **2000**, *246*, 1–11. [[CrossRef](#)]
54. Beake, B.D. The influence of the H/E ratio on wear resistance of coating systems—Insights from small-scale testing. *Surf. Coat. Technol.* **2022**, 128272. [[CrossRef](#)]
55. Beake, B.D.; Vishnyakov, V.M.; Harris, A.J. Nano-scratch testing of (Ti,Fe)N<sub>x</sub> thin films on silicon. *Surf. Coat. Technol.* **2017**, *309*, 671–679. [[CrossRef](#)]
56. Sousa, V.F.C.; Silva, F.J.G.; Alexandre, R.; Fecheira, J.S.; Silva, F.P.N. Study of the wear behaviour of TiAlSiN and TiAlN PVD coated tools on milling operations of pre-hardened tool steel. *Wear* **2021**, *476*, 203695. [[CrossRef](#)]